ISTITUTO NAZIONALE DI FISICA NUCLEARE

INFN/AE-83/6
Luglio 1983

M. Basile, J. Berbiers, G. Bonvicini, G. Cara Romeo, L. Cifarelli, A. Contin, M. Curatolo, G. D'Ali, C. Del Papa, B. Esposito, P. Giusti, T. Massam, R. Nania, G. Natale, F. Palmonari, G. Sartorelli, M. Spinetti, G. Susinno, L. Votano and A. Zichichi:

NEW ISR PHYSICS: HEAVY FLAVOURS AND MULTIHADRONIC FINAL STATES

Paper presented, by A. Zichichi, at the "Seventh International Conference on Experimental Meson Spectroscopy", Brookhaven, April 14-16, 1983

Servizio Documentazione
dei Laboratori Nazionali di Frascati

NEW ISR PHYSICS: HEAVY FLAVOURS AND MULTIHADRONIC FINAL STATES

M. Basile, J. Berbiers, G. Bonvicini, G. Cara Romeo, L. Cifarelli, A. Contin, M. Curatolo, G. D'Alì, C. Del Papa, B. Esposito, P. Giusti, T. Massam, R. Nania, G. Natale, F. Palmonari, G. Sartorelli, M. Spinetti, G. Susinno, L. Votano and A. Zichichi

CERN, Geneva, Switzerland
Istituto di Fisica dell'Università, Bologna, Italy
Istituto Nazionale di Fisica Nucleare, Bologna, Italy
Istituto Nazionale di Fisica Nucleare, LNF, Frascati, Italy

(Presented by A. Zichichi)

TABLE OF CONTENTS

1. - INTRODUCTION

2. - HEAVY FLAVOURS

2. 1. - A brief review of heavy flavours production in hadronic machines

2. 1. 1. - Production cross sections
2. 1. 2. - The "Leading" effect
2. 1. 3. - Further comments
2. 1. 4. - Conclusions

2. 2. - Expected new heavy flavoured states

2. 2. 1. - Examples from previous experience with $SU(3)_{uds}$ and $SU(4)_{udsc}$
2. 2. 2. - Note on the semi-leptonic decay modes: generalized Cabibbo mixing

2. 3. - Cross section estimates: how to go from strangeness to charm, beauty, top and superbeauty

2. 4. - The study of the lepton charge asymmetry and its energy dependence as a way to detect the heaviest flavoured states (baryonic and antibaryonic) at the ($p\bar{p}$) collider.

2. 4. 1. - The total cross sections
2. 4. 2. - The decay branching ratios
2. 4. 3. - The production distributions of baryon and meson states
2. 4. 4. - The relative yield of mesons and baryons
2. 4. 5. - The lepton decay distributions
2. 4. 6. - Estimates of the Asymmetry A^o
2. 4. 7. - Background evaluation
2. 4. 8. - Estimate of the Asymmetry parameter inclusive of background
2. 4. 9. - A detailed case

2. 5. - Comparison with preliminary data from the CERN ($p\bar{p}$) Collider

2. 6. - Conclusions

3. - MULTIHADRONIC FINAL STATES

3. 1. - Introduction and the "Leading" effect

3. 2. - The end of a myth : the high p_T physics

3. 3. - The identification of the correct variables

3. 3. 1. - Experimental results
3. 3. 2. - Conclusions

4. - CONCLUSIONS

REFERENCES

1. - INTRODUCTION

A systematic study of (pp) interactions at the ISR[1-46] has produced two important results :

a) One is in the field of Heavy Flavours production. Here the relevance of the data obtained at the ISR is in the consequences of the physics wich can be done at the collider: the problem of searching for new, very heavy flavours. It will be shown that, if the mechanism of heavy-flavour production at the ISR holds true up to collider energies, a basic new quantity should be measured at the CERN collider: namely, the (e^+/e^-) asymmetry and its energy dependence. The down-like or up-like nature of the heavy flavours produced is reflected in the sign of the (e^+/e^-) asymmetry. The mass difference between the down-like and the up-like states determines the energy dependence of the asymmetry.

b) The other is in the domain of Multihadronic Final States. It will be shown that in order to compare the final states produced in different reactions, such as (pp), (e^+e^-), and (DIS), it is necessary, first of all, to use the correct variables. Once this is done, these processes, so far considered as basically different, can be brought to a common basis of comparison, and striking similarities do emerge.

The detailed discussion of the results, obtained by the BCF group in these two basic fields of purely hadronic interactions, is the content of the present paper.

2. - HEAVY FLAVOURS

The present status of our knowledge on quarks and leptons may be summarized as follows :

Families :	1^{st}	2^{nd}	3^{rd}
Quarks :	$\begin{pmatrix} u \\ d \end{pmatrix}$	$\begin{pmatrix} c \\ s \end{pmatrix}$	$\begin{pmatrix} ? \\ b \end{pmatrix}$
Leptons :	$\begin{pmatrix} \nu_e \\ e \end{pmatrix}$	$\begin{pmatrix} \nu_\mu \\ \mu \end{pmatrix}$	$\begin{pmatrix} \nu_\tau \\ \tau \end{pmatrix}$

There are very good reasons to believe that our knowledge is far from being complete and thus the search for new heavy flavours and the study of their family structure is one of the key problems in Subnuclear Physics.

Let me quote two "theoretical" arguments in favour of further needs of new quarks. The ABJ anomaly cancellation requires that the number of leptons be equal to the number of quarks. This means that a sixth quark is needed. Its natural location would be the up-like member of the 3rd family, i. e. the "top" quark.

According to SuperSymmetry, a very heavy quark with a mass in the few $10^2\,GeV/c^2$ range is needed in order to produce radiatively (see Fig. 1) a gluino with a mass such as to avoid a conflict with existing lower limits[47]. None of the presently known quarks (s, c and b) is heavy enough for this purpose.

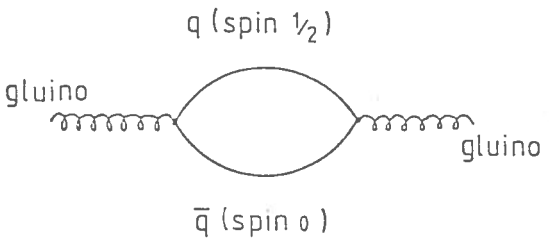

Fig. 1. The diagram illustrates how a gluino can acquire a mass from radiative processes, where a spin 1/2 quark and a spin 0 antiquark are virtually produced. The quark mass must be in the $10^2\,GeV/c^2$ range, in order to allow a gluino mass of the order of a few GeV/c^2.

Apart from these theoretical arguments we should not underestimate that Nature has often provided physicists with more regularities than needed (for example the equality between the proton and the electron charges, which took more than three decades to be understood).

We propose to consider the ratio between the masses of the known heavy quarks as a limit for the regularity in their masses. There are good reasons[48] to consider the strange quark heavy enough to be used in our argument.

At present we know that:

i) $(m_c/m_s) \cong (1.8/0.5) \cong 3.5 \cong 4$;

ii) $(m_b/m_s) \cong (5.5/0.5) \cong 11 \cong 10$.

Suppose that (i) and (ii) are of general validity, i. e. :

$$(m_c/m_s) = [m(\text{uplike quark})/\,m(\text{downlikequark})] = 4\,, \qquad (1)$$

and

$$(m_b/m_s) = [m(\text{family } N+1)/\,m(\text{family } N)] = 10. \qquad (2)$$

We ignore the 1st family (u, d) because of its very light mass. On the other hand, the ratios (1) and (2) would not be inconsistent with the various models used to derive from bound states the masses of these quarks.

The validity of (1) and (2) would allow to conclude that the "top" mass is in the $20\,GeV/c^2$ range. This is too light for SuperSymmetric

models to avoid a gluino mass in conflict with experimental data. On the other hand, SuperSymmetry tells us that the maximum number of flavours, n_f, allowed in order to have a consistent theory (for example: the unification limit not above the Planck mass) is $n_f = 8$. This means that the maximum number of families is 4. In the theories that ignore SuperSymmetry, the asymptotic freedom is lost if $n_f > 16$.

What is not forbidden, in Nature, does take place. Thus, the message from SuperSymmetry is twofold:

i) four families of quarks are allowed;
ii) quarks heavier than (d, u, s, c, b and t) are needed.

Formulas (1) and (2) tell us that the 4^{th} family would have the heavy masses wanted by SuperSymmetry. In fact, using (2), the heavy down-like quark (called, in the following, "superbeauty" or sb) would have a mass in the 50 GeV/c^2 range:

$$m(\text{down-heavy}) = m(\text{"superbeauty"}) \cong 10 \times 5.5 \cong 55 \text{ GeV}/c^2,$$

and, using (1), the heavy up-like quark would have a mass in the 200 GeV/c^2 range:

$$m(\text{up-heavy}) = m(\text{"supertruth"}) \cong 55 \times 4 \cong 220 \text{ GeV}/c^2.$$

The up-like quark of the 4^{th} family should be called "supertruth". In fact, this very heavy mass is wanted by SuperSymmetry; moreover, if SuperSymmetry is a good theory, the 4^{th} family should really be the last of the quark families, ever to be discovered.

The four families are shown in the next graph, where the main objectives of this first part of my talk are indicated by the dotted circles.

Families:	1^{st}	2^{nd}	3^{rd}	4^{th}
Quarks:	$\begin{pmatrix} u \\ d \end{pmatrix}$	$\begin{pmatrix} c \\ s \end{pmatrix}$	$\begin{pmatrix} (t) \\ b \end{pmatrix}$	$\begin{pmatrix} u_H \\ (d_H) \end{pmatrix}$
Leptons:	$\begin{pmatrix} \nu_e \\ e \end{pmatrix}$	$\begin{pmatrix} \nu_\mu \\ \mu \end{pmatrix}$	$\begin{pmatrix} \nu_\tau \\ \tau \end{pmatrix}$	$\begin{pmatrix} \nu_H \\ L_H \end{pmatrix}$

Let us come to a key question: are "top" and "superbeauty" accessible to ($p\bar{p}$) Collider energies? If yes, how can they be detected?

Many methods have been suggested:

i) detection of a hidden state with the study of the invariant mass of the lepton pairs;
ii) detection of an open state with the identification of hadronic decay channels;

iii) study of multilepton events ;
iv) study of the inclusive transverse momentum spectrum of the leptons from semileptonic decays ;
v) study of the transverse dilepton (l, ν) and jets masses.

All of these methods present, in various degrees, experimental problems related to small production cross sections, low global branching ratios, high background levels, poor experimental resolution of the quantities needed to be measured. Moreover, most of them have big troubles in being able to identify the up-like or down-like nature of the new flavours.

We present here a new method to observe the production of heavy mass states, either up-like ("top") or down-like ("superbeauty") which is based on the "Leading" baryon production mechanism, extended to the heaviest baryon and antibaryon states. In fact, due to this production mechanism, a charge asymmetry of the leptons, originating from these heavy flavours can be observed in a selected region of the phase space. Moreover, this asymmetry will show an energy dependence characteristic of the masses of the decaying states.

More precisely, the "top" baryonic state will decay semileptonically into ℓ^+ and produce a positive asymmetry in the outgoing proton rapidity hemisphere

$$A_p = (\ell^+ - \ell^-)/(\ell^+ + \ell^-) = \text{positive}.$$

The "anti-top" antibaryonic state will produce a negative asymmetry in the outgoing antiproton rapidity hemisphere

$$A_{\bar{p}} = (\ell^+ - \ell^-)/(\ell^+ + \ell^-) = \text{negative}.$$

The signs of these asymmetries will be reversed for the "superbeauty" case.

The energy range where to measure the ℓ^{+}_{-} asymmetry, and the separation between the maxima, depend on the parent-daugther mass difference in the decay of the two new flavours. Extending the validity of the generalized Cabibbo mixing (GCM) to the 4^{th} family, the mass differences in the superbeauty and top decays would be:

$$\Delta m = m(\text{top}) - m(\text{beauty}) \cong 20\ \text{GeV}/c^2,$$

$$\Delta m = m(\text{superbeauty}) - m(\text{top}) \cong 30\ \text{GeV}/c^2.$$

The ℓ^{+}_{-} transverse momentum spectra associated with "top" and "superbeauty" will be quite different because:

$$m(\text{"top"}) \cong 25\ \text{GeV}/c^2\ ,$$

$$m(\text{"superbeauty"}) \cong 55\ \text{GeV}/c^2,$$

thus the Asymmetry will change sign with increasing lepton energy.

Fig. 2 shows the main trend of the measurement we propose. Notice that this GCM condition, if not valid, would not spoil our method. It would only shift the energy spectrum of e^- from superbeauty decay to higher values.

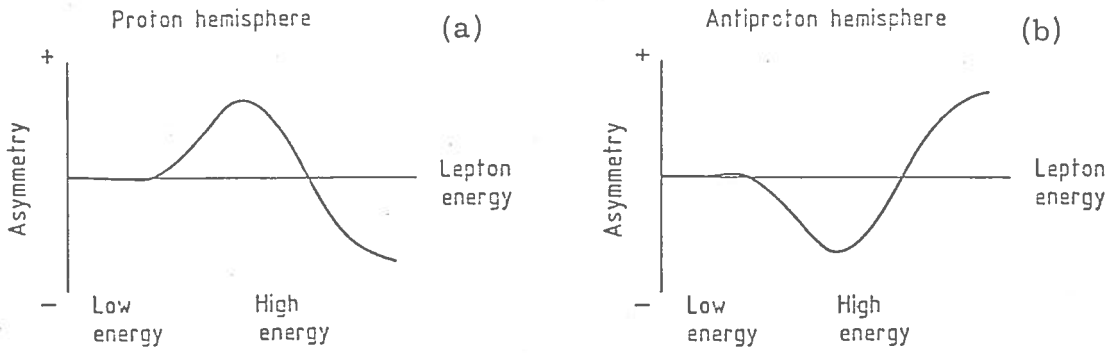

Fig. 2. Main trend of the electron charge Asymmetry in the proton hemisphere (a) and in the antiproton hemisphere (b).

As we will see in the following, the amplitude of the effect depends on:

i) production cross sections;
ii) production and decay, angular and momentum distributions;
iii) branching ratios into semileptonic channels;
iv) luminosity;
v) acceptance and rejection power of the experimental set-up designed to observe the leptons produced by these "new" flavours decay.

2.1. - A brief review of heavy flavours production in hadronic machines.

How to look for "top" and "superbeauty" at the ($p\bar{p}$) Collider, is a problem analogous to "charm" and "beauty" in hadronic machines and, in particular, at the ISR. It is probably instructive to review, very briefly, the main steps in this field.

2.1.1. - Production cross sections.

The theoretical predictions for the charm production cross section and the experimental findings are shown in Table I.

If we were to believe in the string model or in the statistical thermodynamical model, or in the first QCD attempts (fusion model), the conclusion should have been that the production and observation of "charm" is out of question in hadronic machines.

Only recently QCD models (flavour excitation) came nearer to experimental findings. In Fig. 3 all the experimental data are shown and compared with the various steps in the QCD models. Notice that neither

ln(s) nor $\ln^2(s)$ are compatible with the observed threshold behaviour.

Table I - Charm cross section at ISR energies ($\sigma_\pi = 10^2$ mb).

String model	: 10^{-10}	x σ_π
Fermi-Hagedorn	: 10^{-5}	x σ_π
QCD (Fusion)	: 10^{-4}	x σ_π
QCD (Flavour excitation)	: $10^{-2} - 10^{-3}$	x σ_π
Experimentally	: = 10^{-2}	x σ_π

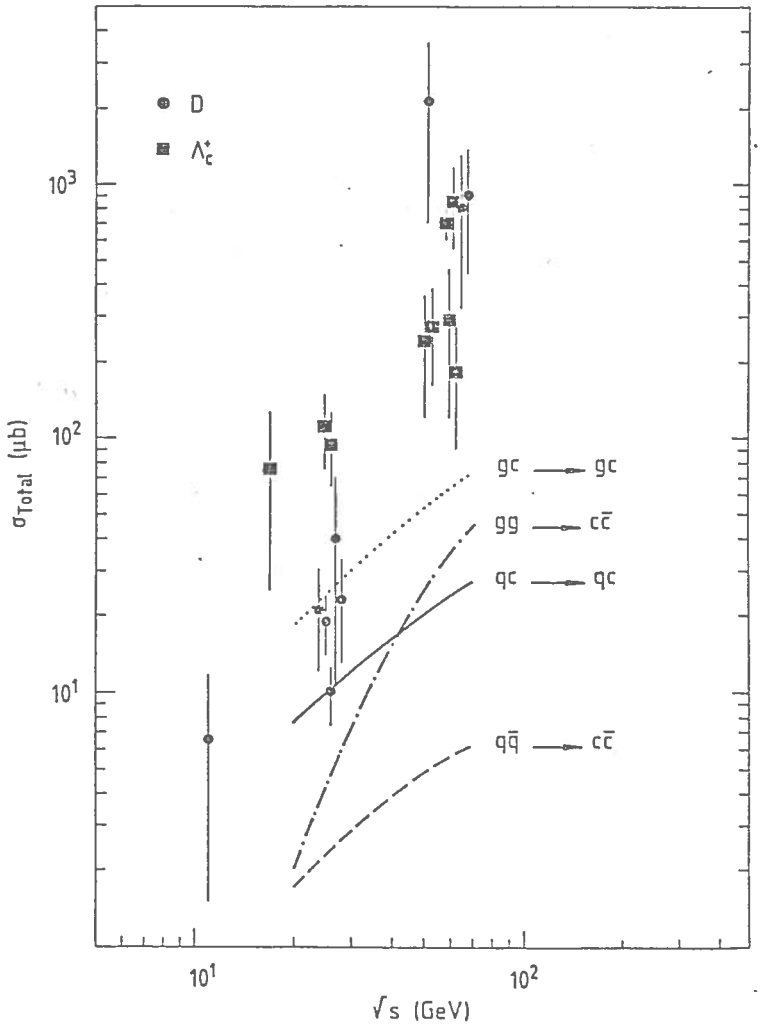

Fig. 3. Cross sections expected on the basis of gluon and quark fusion models ($gg \to c\bar{c}$ and $q\bar{q} \to c\bar{c}$ curves). Other QCD models are also shown. The data are taken from refs. 1, 7, 14 and 49.

2. 1. 2. - The "Leading" effect.

A result which was theoretically unpredicted is the "Leading" effect which shows up in the production of heavy flavours.

A detailed study of (pp) interactions at the ISR showed that the Λ_c^+ is produced in a "Leading" way[3].

After this experimental result was obtained, a series of theoretical proposals were presented, to account for the "Leading" Λ_c^+ production. The longitudinal momentum distribution[3] for Λ_c^+ was in fact found at the ISR to be:

$$(d\sigma/d|x|) \sim (1 - |x|)^{\alpha} \qquad \text{with} \qquad \alpha = 0.40 \pm 0.25 .$$

The results are shown in Fig. 4a. The charmed meson production[15] was on the other hand measured to be "non-Leading", i. e.

$$E(d\sigma/d|x|) \sim (1 - |x|)^{\alpha} \qquad \text{with} \qquad \alpha \approx 3 .$$

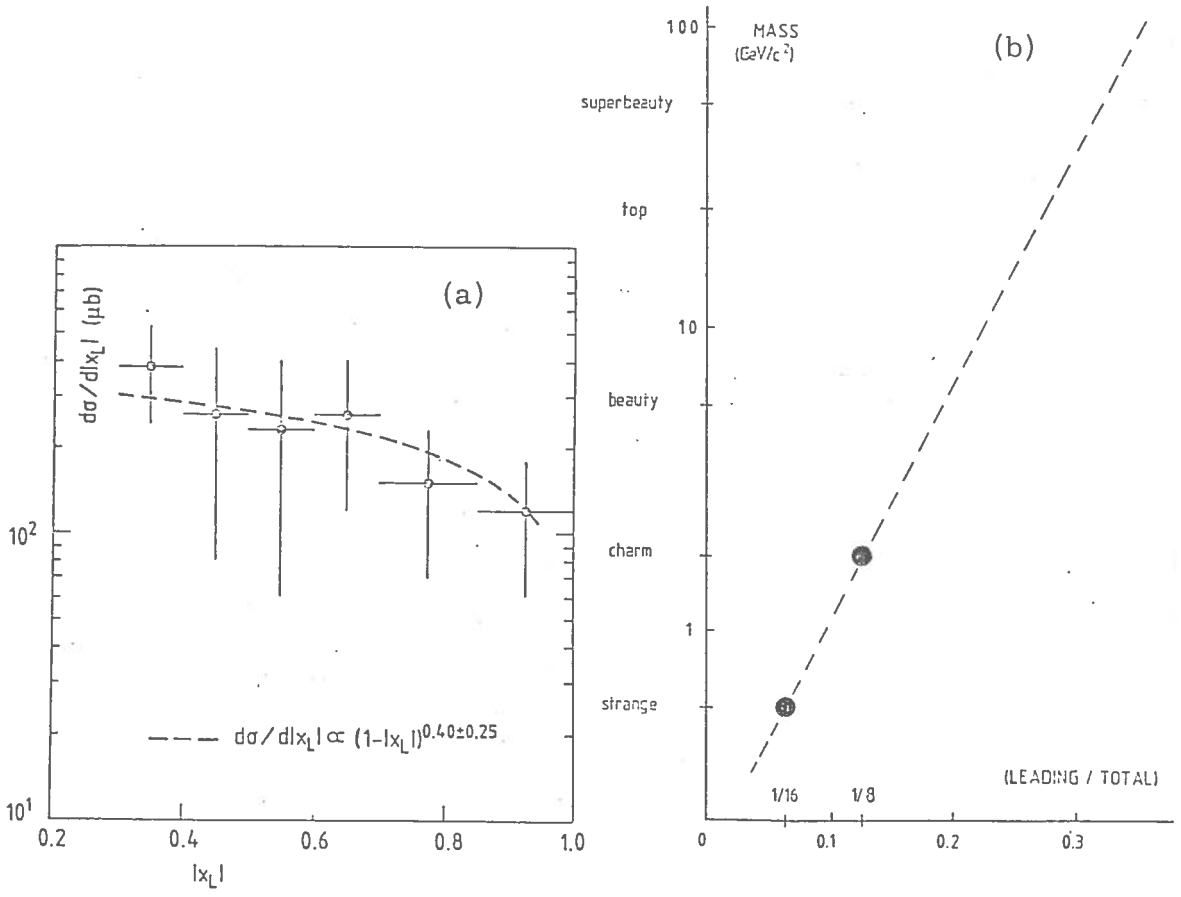

Fig. 4. (a) Experimental longitudinal momentum distribution of Λ_c^+; (b) Qualitative behaviour of the quantity (Leading/Total) as a function of the quark mass, at $\sqrt{s}$ = 62 GeV.

This can be "a posteriori" qualitatively understood in terms of the Λ_c^+ obtained by a recombination of the spectator c-quark with a valence (ud) pair in the proton; while the $\bar{D}$ production is given by the recombination of the spectator $\bar{c}$-quark with a most one valence quark [50, 51].

Figure 4b shows the qualitative behaviour, as a function of the quark mass, of the quantity (Leading/Total), which will be defined in section 2. 4. 4 as the ratio between the inclusive cross-section for producing leading baryons in one hemisphere and the total cross-section for producing $(q\bar{q})$ pairs. This figure shows that, at least at the ISR energies, the "Leading" production increases with increasing quark mass.

A more complete summary of charm production in purely hadronic interactions is reported in the Table II. There is no model which can fit all measured quantities.

Table II

	experiment	models		
		diffractive	flavour excitation	fusion
Leading effect	yes	yes	yes	no
threshold behaviour	steeper than $\ln^2 s$	$\ln s$	steeper than $\ln^2 s$	>> steeper than $\ln^2 s$
mass dependence	?	$1/m^2$	stronger than $1/m^2$	>> stronger than $1/m^2$
cross section	large	large	large	small
A^α dependence	$\alpha < 2/3$ (*)	$\alpha = 2/3$	$\alpha = 1$	α = ...

(*) The p_T dependence is derived from data on strangeness.

2. 1. 3. - Further comments.

For those who have strong faith on QCD it could be interesting to extend our review. In fact the photoproduction was considered a simpler case for QCD. Therefore its predictions should have been in aggreement with experimental findings.

A summary of QCD problems in photoproduction physics is as follows:

a) large photoproduction cross sections of the Heavy Flavours are impossible to be predicted by perturbative QCD;
b) the p_T dependence of inelastic ($c\bar{c}$), for open and hidden states, cannot be accounted for by QCD;
c) the A-dependence cannot be A^1.

2. 1. 4. - Conclusions.

The conclusion of this short review on the "charm" flavour production in (pp) interactions is therefore:

i) the cross section values found are at least an order of magnitude above the "theoretical" predictions of perturbative QCD;
ii) the x-distribution for Λ_c^+, i. e. the "Leading" effect, was theoretically unpredicted;
iii) with "new" models (essentially flavour excitation[51, 52] and non-perturbative QCD[50]) both cross sections values and x-distributions can be "theoretically" derived.

All this should be quite a warning for QCD prediction on Heavy Flavours production at extreme energies such as those of the ($p\bar{p}$) CERN Collider.

2. 2. - Expected new heavy flavoured states.

The main purpose of this section is to call attention on the enormous number of new states which are expected on the basis of the old and new flavours.

2. 2. 1. - Examples from previous experience with $SU(3)_{uds}$ and $SU(4)_{udsc}$.

The following graph illustrates what could indeed happen.

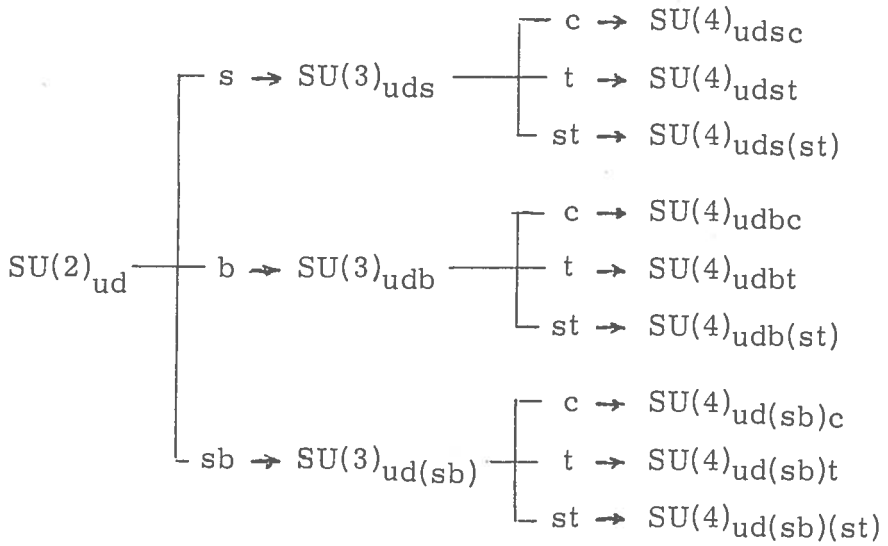

With 3 flavours (u, d and s) the famous $SU(3)_{uds}$ came out. It could be that "beauty" will produce another $SU(3)_{udb}$. The advent of the "charm" with four flavours (udsc) produced $SU(4)_{udsc}$. On the other hand with the "top" there are two possible SU(4): $SU(4)_{udst}$ and $SU(4)_{udbt}$.

Despite the large mass differences among the various flavours, it could be that Nature will provide, as usual, more regularities than wanted. The above global symmetry groups for the structure of the various possible particle states could eventually show up, even if not expected.

If "superbeauty" was there we would have even a larger set of SU(3) and of SU(4) states, in addition to all combination of purely singlets like (s, c, b, t and sb).

Examples of SU(4) structures using (u, d, s, c, b, sb and supertruth) are presented in Figs. 5 to 7. They include mesonic and baryonic states.

If we enlarge the symmetries to the intrinsic spins the multitude of states increases further. These are indicated, for the first 3 flavours (u, d and s), in the Tables III and IV, respectively for the mesons and for the baryons in SU(6).

Table III - SU(6) mesonic supermultiplets.

SU(6)	$SU(3)_f$	J^{PC}	Particle states	Number of states
$[(35 \oplus 1) \otimes 1]$; (L = 0)	$8 \oplus 1$	0^{-+}	π, K, η, η'	36
	$8 \oplus 1$	1^{--}	ϱ, K^*, ω, ϕ	
$[(35 \oplus 1) \otimes 3]$; (L = 1)	$8 \oplus 1$	1^{+-}	B, $Q_{1,2,\ldots,?}$	108
	$8 \oplus 1$	0^{++}	S, χ, S^*, ε	
	$8 \oplus 1$	1^{++}	A_1, $Q_{1,2}$, D, E	
	$8 \oplus 1$	2^{++}	A_2, K^{**}, f, f'	

An example of how the multitude of the states goes with the mass is shown in Figs. 8a and 8b, where the masses of the particles run from few GeV/c^2 up to 60 GeV/c^2.

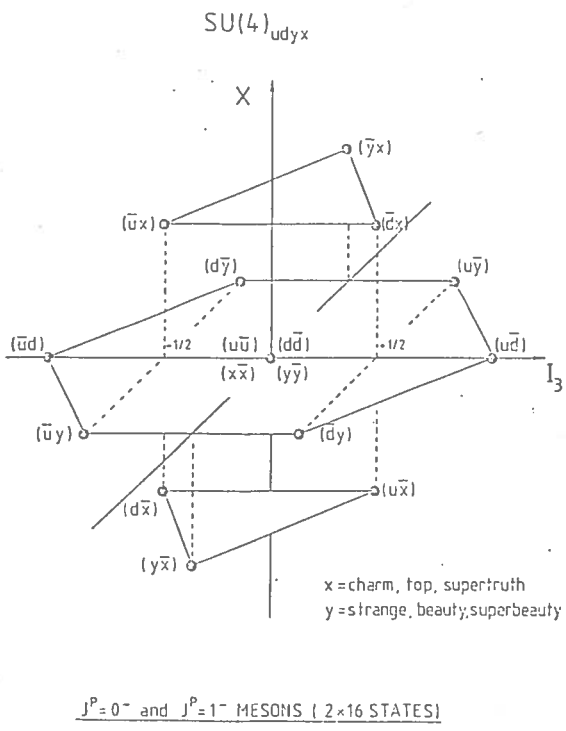

Fig. 5. The $SU(4)_f$ mesonic multiplets for $J^P = 0^-$; the same multiplet structure repeats for $J^P = 1^-$. "x" represents the quarks with electric charge +2/3, "y" the quarks with electric charge -1/3. Each of the possible udyx combinations should produce an $SU(4)_f$. The quark composition for each state is indicated in parenthesis.

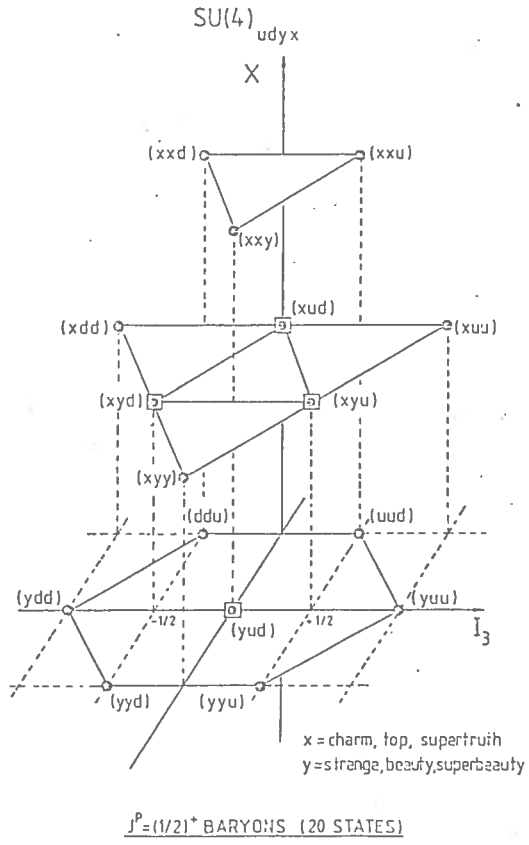

Fig. 6. Showing the structure of the expected baryonic $J^P = 1/2^+$ $SU(4)_f$ 20-plets.

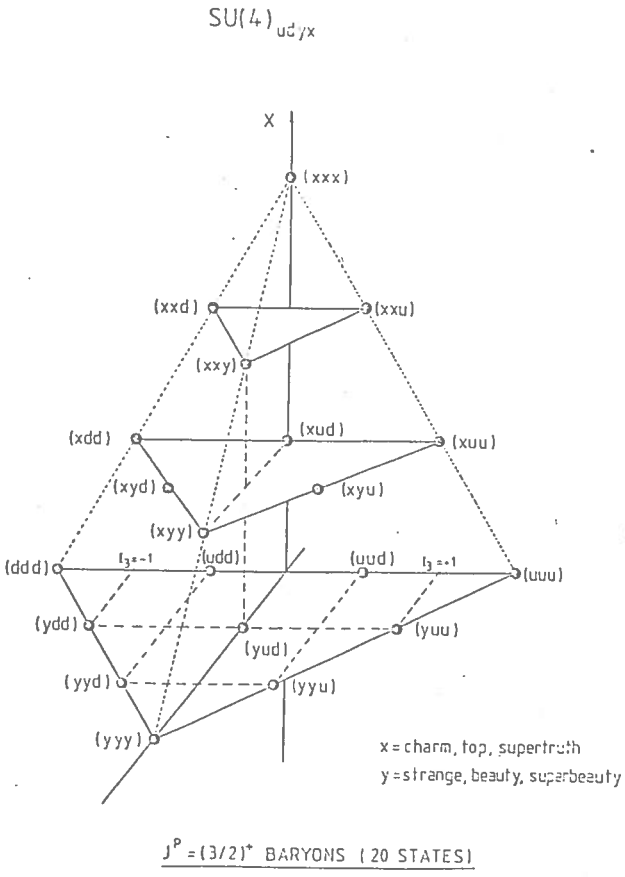

Fig. 7. Showing the structure of the expected baryonic $J^P = 3/2^+$ $SU(4)_f$ 20-plets.

Table IV - Baryons in SU(6) supermultiplets.

$[SU(6), L^P]$	$SU(3)_f$	J^P	Standard names of particle states	
$(56, 0^+)$	8	$1/2^+$	N, Λ, Σ, Ξ	
	10	$3/2^+$	N^*, Σ^*, Ξ^*, Ω^-	
$(70, 1^-)$	1	$1/2^-$	Repeat singlet	Repeat means that the quantum numbers (isospin and strangeness) of the states are identical to the "octet" and "decuplet" already known for the 56-case.
	8	$1/2^-$	Repeat octet	
	10	$1/2^-$	Repeat decuplet	
	1	$3/2^-$	Repeat singlet	
	8	$3/2^-$	Repeat octet	
	10	$3/2^-$	Repeat decuplet	
	8	$1/2^-$	Repeat octet	
	8	$3/2^-$	Repeat octet	
	8	$5/2^-$	Repeat octet	

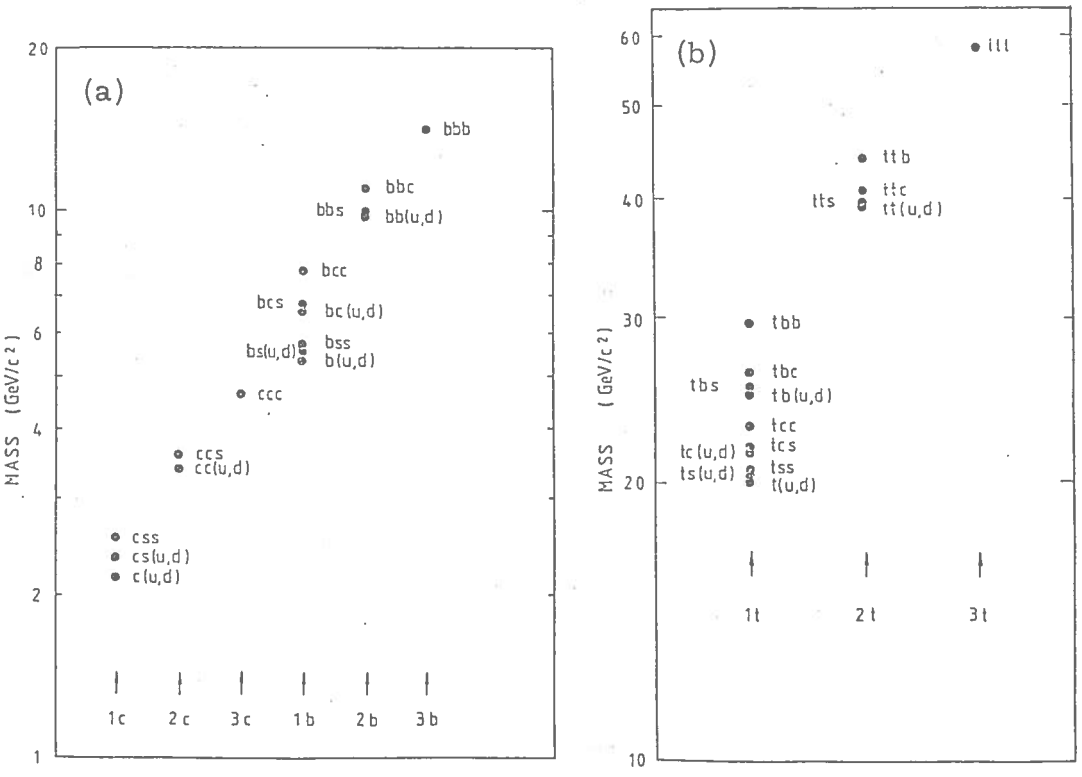

Fig. 8. The figure shows the mass ranges of the baryon states with: (a) from 1 to 3 charm or beauty quarks; (b) from 1 to 3 top quarks.

2. 2. 2. - Note on the semi-leptonic decay modes : generalized Cabibbo mixing.

A fact of Nature is that the matrix which relates the down-like "weak" flavours "Cabibbo mixed"

$$\begin{pmatrix} d_c \\ s_c \\ b_c \end{pmatrix}$$

to the "strong" flavours

$$\begin{pmatrix} d \\ s \\ b \end{pmatrix}$$

is approximately a unit matrix

$$\begin{pmatrix} d_c \\ s_c \\ b_c \end{pmatrix} \simeq \begin{pmatrix} 1 & 0 & 0 \\ 0 & 1 & 0 \\ 0 & 0 & 1 \end{pmatrix} \begin{pmatrix} d \\ s \\ b \end{pmatrix}$$

as shown in Figs. 9a and 9b.

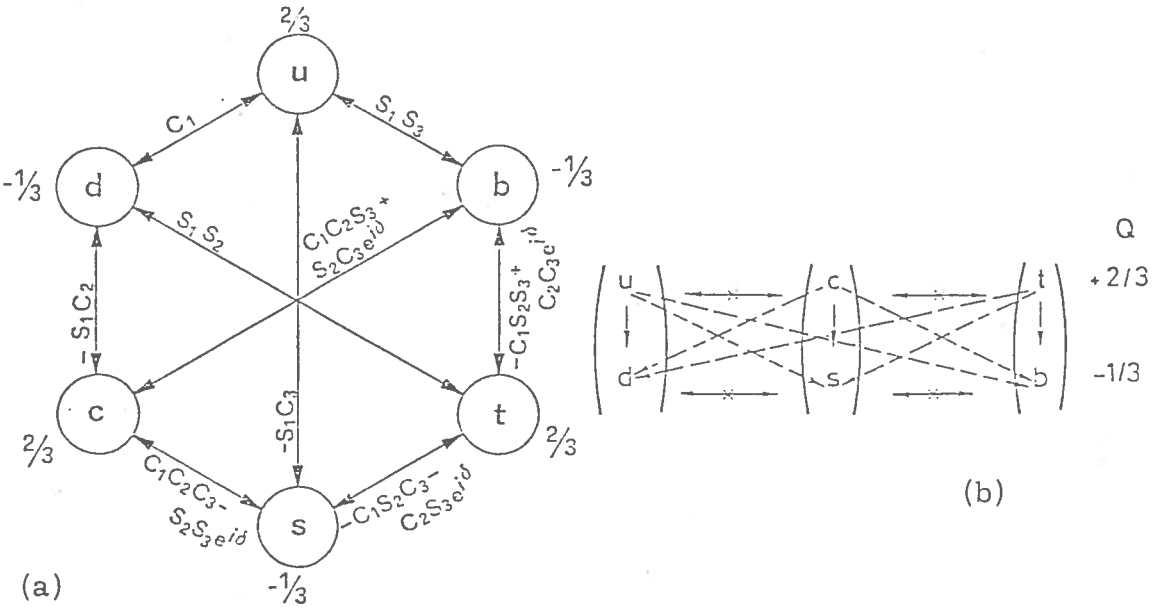

Fig. 9. (a) The six quark mixing with CP violation. $S_i = \sin\theta_i$, $C_i = \cos\theta_i$. (b) Transitions among the various states. The Cabibbo mixing opens the dashed channels. The horizontal transitions are forbidden for any value of the mixing angle. Allowed neutral currents are: $u\bar{u}$, $c\bar{c}$, $t\bar{t}$, $d\bar{d}$, $s\bar{s}$ and $b\bar{b}$.

In order to extend the generalized Cabibbo mixing to the 4th Family, we make the following extrapolations:

i) all the generalized Cabibbo angles, even those coming from the existence of the 4th family are small;
ii) the flavour-changing neutral currents are forbidden to any order of family;
iii) the amplitude for the transition from family N to family $N \pm \alpha$ has a coefficient

$$\prod_{i=1,\alpha} (\sin \theta_i) .$$

As a consequence, the Cabibbo-favoured decay chains of flavours c, b, t and sb are:

$$\begin{aligned} c &\to s \\ b &\to c \to s \\ t &\to b \to c \to s \\ sb &\to t \to b \to c \to s . \end{aligned}$$

All we need to know is the charge sign of the lepton in a transition from an "up-like" to a "down-like" flavour and viceversa. This can be summarized as follows:

$$\begin{matrix} \binom{u}{d} & \binom{c}{s} & \binom{t}{b} & \binom{st}{sb} \\ \Downarrow & \Downarrow & \Downarrow & \Downarrow \\ \binom{1}{2} & \binom{3}{4} & \binom{5}{6} & \binom{7}{8} \end{matrix} \quad \begin{matrix} \\ \\ \leftarrow \text{ ODD (= UP-LIKE) QUARKS} \\ \leftarrow \text{ EVEN (= DOWN-LIKE) QUARKS} \end{matrix}$$

with the charge formula written as:

$$Q = (1/3 + f_i)/2$$

with:

$f_i = +1$ for odd quarks $(i = 1, 3, 5, 7)$
$f_i = -1$ for even quarks $(i = 2, 4, 6, 8)$.

From this follows the electric charge sign of the lepton in the semileptonic decay of the flavour:

ODD → EVEN (UP-LIKE → DOWN-LIKE)
TRANSITION ⇒ POSITIVE LEPTON

EVEN → ODD (DOWN-LIKE → UP-LIKE) TRANSITION →
⇒ NEGATIVE LEPTON

As will be seen in the Fig. 15, a sequence $t \to b \to c \to s$ will be accompained by the semileptonic series giving rise to $e^+ \to e^- \to e^+$. For the antiquark sequence $\bar{t} \to \bar{b} \to \bar{c} \to \bar{s}$, the charges will be reversed ($e^- \to e^+ \to e^-$). These results are straightforward consequencies of the previous table.

2. 3. - Cross section estimates : how to go from strangeness to charm, beauty, top and superbeauty.

Now comes a key question: once we know the "strange" and "charm" cross sections, is it possible to predict the heavier flavours (c, b, t or sb) cross sections in hadronic collisions?

Simple arguments bring to the conclusion that:

$$\sigma(m) \sim (1/m^2) \times f(s/m^2). \qquad (3)$$

In fact, the only quantities which enter in the problem of producing a $(q\bar{q})$ pair, having at disposal the total energy $\sqrt{s}$, are the quark mass, m, and the total energy, $\sqrt{s}$.

Formula (3) is based on dimensional and scaling arguments:

- Dimension says that: $\sigma \sim (1/m^2)$;
- Scaling says that the two quantities m^2 and s are such that nothing changes if their ratio (s/m^2) is kept constant; the ratio (s/m^2) is the dimensionless quantity needed if no other scale should remain in the game.

The basic formula is therefore:

$$\sigma_i\left[(\sqrt{s})_{pp} = E_i\right] = (m_j/m_i)^2 \times \sigma_j\left[(\sqrt{s})_{pp} = E_j = (m_j/m_i)E_i\right] \qquad (4)$$

where:

σ_i, σ_j are the production cross sections,

m_i, m_j are the masses,

E_i, E_j are the energies,

at which flavours f_i and f_j are produced.

The results are shown in Figs. 10-13, where we have used:

i) the strangeness data to predict c, b, t and sb;
ii) the "charm" data to predict b, t and sb;
iii) the "beauty" data to predict t and sb.

Finally, for completeness, we also report the most recent QCD predictions of refs. 50 and 51 (Fig. 14).

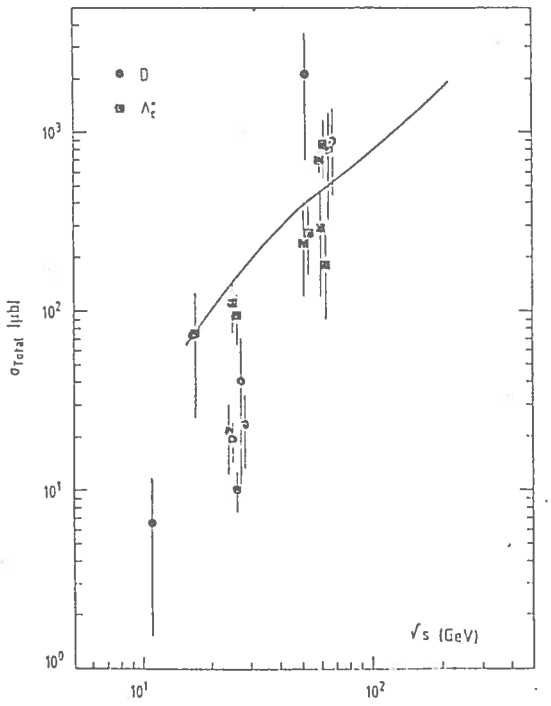

Fig. 10. Charm cross section derived from strange cross section following formula (4).

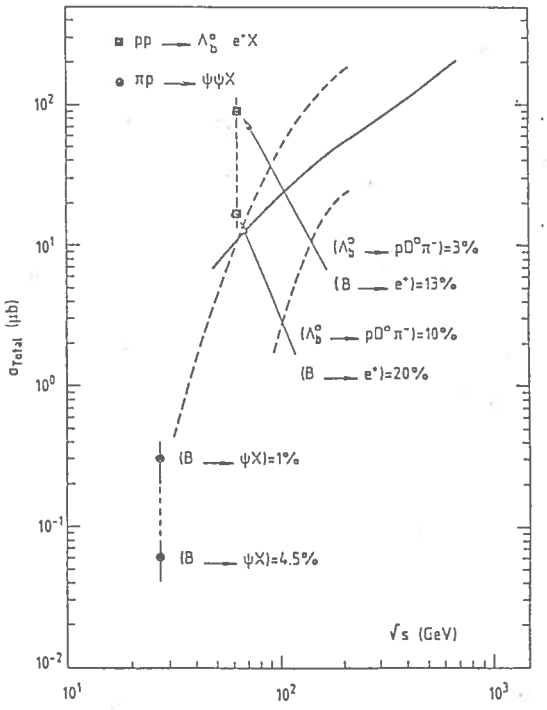

Fig. 11. Beauty cross section derived from strange (full line) and charm (dashed lines - notice the width due to the experimental uncertainties) cross sections following formula (4). The data are taken from refs. 8 and 53.

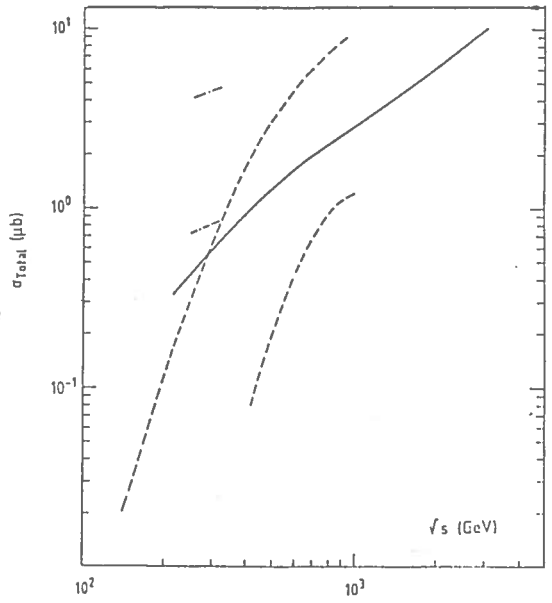

Fig. 12. Top cross section derived from strange (full line), charm (dashed lines) and beauty (dash/point lines) cross sections following formula (4).

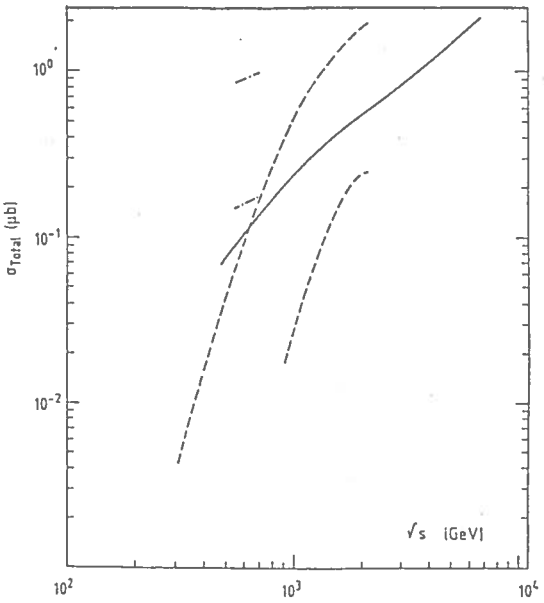

Fig. 13. Superbeauty cross section derived from strange (full line), charm (dashed lines) and beauty (dashed-dotted lines) cross sections following formula (4).

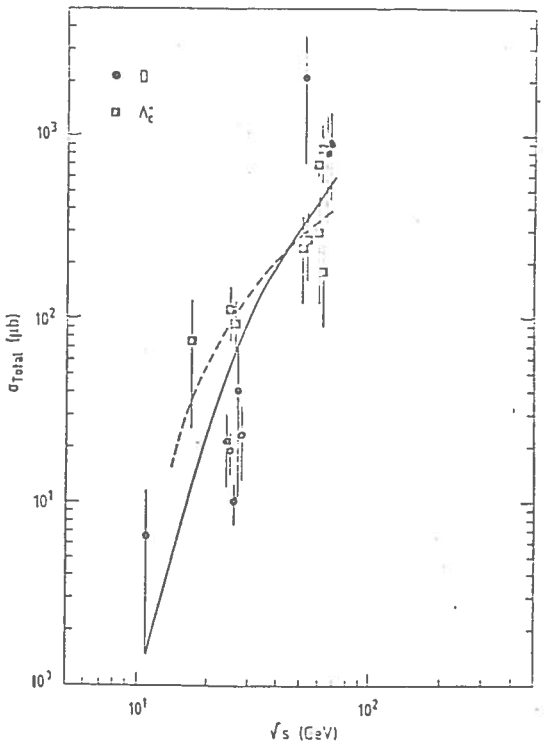

Fig. 14. Non perturbative QCD predictions (dashed line) and flavour excitation perturbative QCD predictions (full line) for charm hadroproduction.

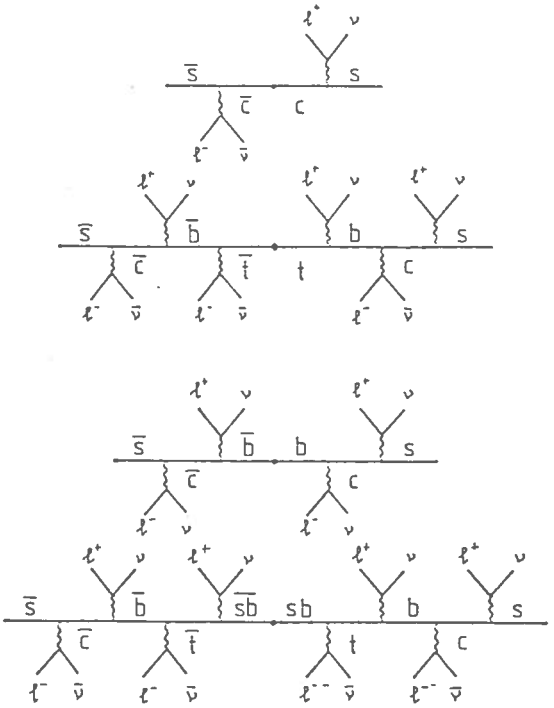

Fig. 15. Diagram illustrating all the possible electric charge signs of the electrons originating from the semileptonic decay of the quarks c, b, t and sb.

2.4. - The study of the lepton charge asymmetry and its energy dependence as a way to detect the heaviest flavoured states (baryonic and antibaryonic) at the ($p\bar{p}$) collider.

The leptonic decay chains, following the generalized Cabibbo dominance, for the various flavours c, b, t, sb, are shown in Fig. 15.

Once a particle-antiparticle pair has been produced, on the average the number of positive and negative leptons from its decay is equal. However we will discuss under which conditions an asymmetry in the number of positive and negative leptons can be observed, due to the different longitudinal momentum production distribution for baryons and mesons, and to the dependence of the lepton p_T spectra from the product particle mass.

Let us define the Asymmetry parameters as

$$A^o(p_T, \theta_{cut}) = \frac{N(\ell^+) - N(\ell^-)}{N(\ell^+) + N(\ell^-)} \qquad (5)$$

where $N(\ell^+) \equiv N(\ell^+; p_T, \theta_{cut})$ and $N(\ell^-) \equiv N(\ell^-; p_T, \theta_{cut})$ are the number of positive and negative leptons produced in the angular range $0^o < \theta < \theta_{cut}$ and with transverse momentum p_T.

The number of positive leptons ℓ^+ is expressed by

$$N(\ell^+) = L\left[n_{sb}(\ell^+) + n_t(\ell^+) + n_b(\ell^+) + n_c(\ell^+)\right]$$

where L is the total integrated luminosity and $n_f(\ell^+)$ (with f = sb, t, b, c) is the contribution from the direct production of sb, t, b, c states.

Analogously the number of negative leptons is given by

$$N(\ell^-) = L\left[(n_{sb}(\ell^-) + n_t(\ell^-) + n_b(\ell^-) + n_c(\ell^-)\right].$$

The leptons originated by the decay of the various flavours and antiflavours are summarized in Tables IV and V.

Table IV

Flavour	Decays producing ℓ^+	Decays producing ℓ^-
sb	$sb \to t \to b + \ell^+$ $sb \to t \to b \to c \to s + \ell^+$	$sb \to t + \ell^-$ $sb \to t \to b \to c + \ell^-$
t	$t \to b + \ell^+$ $t \to b \to c \to s + \ell^+$	$t \to b \to c + \ell^-$
b	$b \to c \to s + \ell^+$	$b \to c + \ell^-$
c	$c \to s + \ell^+$	

Table V

Antiflavour	Decays producing ℓ^+	Decays producing ℓ^-
$\bar{sb}$	$\bar{sb} \to \bar{t} + \ell^+$ $\bar{sb} \to \bar{t} \to \bar{b} \to \bar{c} + \ell^+$	$\bar{sb} \to \bar{t} \to \bar{b} + \ell^-$ $\bar{sb} \to \bar{t} \to \bar{b} \to \bar{c} \to \bar{s} + \ell^-$
$\bar{t}$	$\bar{t} \to \bar{b} \to \bar{c} + \ell^+$	$\bar{t} \to \bar{b} + \ell^-$ $\bar{t} \to \bar{b} \to \bar{c} \to \bar{s} + \ell^-$
$\bar{b}$	$\bar{b} \to \bar{c} + \ell^+$	$\bar{b} \to \bar{c} \to \bar{s} + \ell^-$
$\bar{c}$		$\bar{c} \to \bar{s} + \ell^-$

In order to write down explicity $n_f(\ell^+)$ let us define:

i) $\sigma_f^T \equiv$ total cross section for the production of open $(f, \bar{f})$ pairs;

ii) $\varrho_{Mf}, \varrho_{\bar{M}\bar{f}}, \varrho_{Bf}, \varrho_{\bar{B}\bar{f}} \equiv$ ratio between, the inclusive cross-section for producing (M = meson, $\bar{M}$ = antimeson, B = baryon, $\bar{B}$ = antibaryon) states, and the total cross section σ_f^T;

iii) $BR_{Mf'}, BR_{\bar{M}\bar{f}'}, BR_{Bf'}, BR_{\bar{B}\bar{f}'} \equiv$ semileptonic branching ratio of the various states with flavour f' (f' = c, b, t, sb);

iv) $\varepsilon_{Mf}(\ell^{\pm}_{\bar{f}'}), \varepsilon_{\bar{M}\bar{f}}(\ell^{\pm}_{f'}), \varepsilon_{Bf}(\ell^{\pm}_{\bar{f}'}), \varepsilon_{\bar{B}\bar{f}}(\ell^{\pm}_{\bar{f}'}) \equiv$ acceptance for $\ell^{\pm}$ from the leptonic decay of the flavour f' produced in the decay chain of the state with flavour f. This acceptance is a function of the lepton p_T and of the cut in $\theta < \theta_{cut}$ applied to the lepton polar angle.

Accordingly we have, for the case of "superbeauty":

$$n_{sb}(\ell^+) = \sigma_{sb}^T \Big\{ \varrho_{Msb}\Big[BR_{Mt}\varepsilon_{Msb}(\ell^+_t) + BR_{Mc}\varepsilon_{Msb}(\ell^+_c)\Big] +$$

$$+ \varrho_{\bar{M}sb}\Big[BR_{\bar{M}sb}\varepsilon_{\bar{M}sb}(\ell^+_{\bar{sb}}) + BR_{\bar{M}b}\varepsilon_{\bar{M}sb}(\ell^+_b)\Big] +$$

$$+ \varrho_{Bsb}\Big[BR_{Bt}\varepsilon_{Bsb}(\ell^+_t) + BR_{Bc}\varepsilon_{Bsb}(\ell^+_c)\Big] +$$

$$+ \varrho_{\bar{B}sb}\Big[BR_{\bar{B}sb}\varepsilon_{\bar{B}sb}(\ell^+_{\bar{sb}}) + BR_{\bar{B}b}\varepsilon_{\bar{B}sb}(\ell^+_b)\Big]\Big\}$$

and

$$n_{sb}(\ell^-) = \sigma_{sb}^T \Big\{ \varrho_{\bar{M}sb}\Big[BR_{\bar{M}t}\varepsilon_{\bar{M}sb}(\ell^-_{\bar{t}}) + BR_{\bar{M}c}\varepsilon_{\bar{M}sb}(\ell^-_{\bar{c}})\Big] +$$

$$+ \varrho_{Msb}\Big[BR_{Msb}\varepsilon_{Msb}(\ell^-_{sb}) + BR_{Mb}\varepsilon_{Msb}(\ell^-_b)\Big] +$$

$$+ \varrho_{\bar{B}sb}\Big[BR_{\bar{B}t}\varepsilon_{\bar{B}sb}(\ell^-_{\bar{t}}) + BR_{\bar{B}c}\varepsilon_{\bar{B}sb}(\ell^-_{\bar{c}})\Big] +$$

$$+ \varrho_{Bsb}\Big[BR_{Bsb}\varepsilon_{Bsb}(\ell^-_{sb}) + BR_{Bb}\varepsilon_{Bsb}(\ell^-_b)\Big]\Big\}.$$

The analogous expressions for $n_t(\ell^{\pm})$, $n_b(\ell^{\pm})$, $n_c(\ell^{\pm})$ can be easily derived and are not reported here.

From the above formulas it can be seen that in order to evaluate the Asymmetry parameter A^o one needs to know:

i) the total cross section $\Rightarrow \sigma^T$;

ii) the decay branching ratios $\Rightarrow$ BR;

iii) the production distributions of the baryons or mesons states $\Rightarrow \varepsilon$;

iv) the relative fraction of baryons and mesons $\Rightarrow \varrho$;

v) the lepton distributions in the decays $\Rightarrow \varepsilon$.

We will now discuss in some detail the assumptions we made for these quantities.

2. 4. 1. - The total cross sections.

We will extrapolate the total cross sections for the heavy flavours at the ($p\bar{p}$) Collider energy, $\sqrt{s}$ = 540 GeV, using formula (4) and starting from the strangeness cross section. Using the known masses for "charm" and "beauty" baryons and mesons, and the values:

$$m_t = 25\ \mathrm{GeV}/c^2\ , \qquad m_{sb} = 55\ \mathrm{GeV}/c^2\ ,$$

for the "top" and "superbeauty" particles, one obtains:

$$\sigma_c \approx 2000\ \mu b\ , \tag{6a}$$

$$\sigma_b \approx 140\ \mu b\ , \tag{6b}$$

$$\sigma_t \approx 1.5\ \mu b\ , \tag{6c}$$

$$\sigma_{sb} \approx 0.15\ \mu b\ . \tag{6d}$$

Other estimates, from perturbative QCD, will however be taken into account when discussing the results. It will be shown that, under some conditions, even these very low cross sections ($\sigma_b \simeq 10\,\mu b$ and $\sigma_t \simeq 0.1\,\mu b$)[55] give rise to a measurable Asymmetry.

2. 4. 2. - The decay branching ratios.

Recent data from CLEO[54] give for the semileptonic branching ratio of the "beauty" mesons:

$$(M_b \to \ell^{\pm})/(M_b \to \text{all}) \approx 0.13\ .$$

In our Monte Carlo we assume the known semileptonic branching ratios for "charm":

$$(D \to \ell^{\pm})/(D \to \text{all}) \approx 0.085\ ,$$

$$(\Lambda_c^+ \to \ell^{\pm})/(\Lambda_c^+ \to \text{all}) \approx 0.045\ .$$

and the conservative value of 0.1 for all other heavier particles.

2. 4. 3. - The production distributions of baryon and meson states.

The study of the reactions:

$$pp \rightarrow D + e^- + \text{anything} ,$$

$$pp \rightarrow \Lambda_c^+ + e^- + \text{anything} ,$$

$$pp \rightarrow \Lambda_b^o + e^+ + \text{anything} ,$$

at the ISR, indicate that in baryon-baryon collisions the heavy flavoured baryons are produced according to a rather flat x-distribution:

$$(d\sigma/dx) \sim \text{const.} ,$$

while the heavy flavoured mesons are produced with softer x-distribution of the type:

$$E(d\sigma/d|x|) \sim (1 - |x|)^3 .$$

These distributions will be assumed all along the following discussion, together with the p_T dependence:

$$(d\sigma/dp_T) \sim p_T \exp(-2.5\ p_T)$$

observed at the ISR in the production of heavy flavours[4,16].

2. 4. 4. - The relative yield of mesons and baryons.

From the data on strangeness production at the ISR, it can be assumed that, in (pp) collisions the following reactions dominate

$$pp \rightarrow \bar{M}_{Central} + B_{Leading} + \text{anything} \equiv \{\bar{M}_C; B_L\} ,$$

$$pp \rightarrow \bar{M}_{Central} + M_{central} + \text{anything} \equiv \{\bar{M}_C; M_C\} .$$

In ($p\bar{p}$) collisions, due to the anti-baryonic nature of the p hemisphere, the following reactions can take place:

$$p\bar{p} \rightarrow \bar{M}_{Central} + B_{Leading} + \text{anything} \equiv \{\bar{M}_C; B_L\} ,$$

$$p\bar{p} \rightarrow M_{Central} + \bar{B}_{Leading} + \text{anything} \equiv \{M_C; \bar{B}_L\} ,$$

$$p\bar{p} \rightarrow \bar{M}_{Central} + M_{Central} + \text{anything} \equiv \{\bar{M}_C; M_C\} ,$$

$$p\bar{p} \rightarrow \bar{B}_{Leading} + B_{Leading} + \text{anything} \equiv \{\bar{B}_L; B_L\} .$$

In this case, the ratio of the inclusive cross sections for producing

the four classes of particles M_C, $\bar{M}_C$, B_L and $\bar{B}_L$ and the total cross sections are:

$$\varrho_M = \left[\sigma\{M_C; \bar{B}_L\} + \sigma\{\bar{M}_C; M_C\}\right]/\sigma^T ,$$

$$\varrho_{\bar{M}} = \left[\sigma\{\bar{M}_C; B_L\} + \sigma\{\bar{M}_C; M_C\}\right]/\sigma^T ,$$

$$\varrho_B = \left[\sigma\{\bar{M}_C; B_L\} + \sigma\{\bar{B}_L; B_L\}\right]/\sigma^T ,$$

$$\varrho_{\bar{B}} = \left[\sigma\{M_C; \bar{B}_L\} + \sigma\{\bar{B}_L; B_L\}\right]/\sigma^T ;$$

with

$$\sigma^T = \sigma\{\bar{M}_C; B_L\} + \sigma\{M_C; \bar{B}_L\} + \sigma\{\bar{M}_C; M_C\} + \sigma\{\bar{B}_L; B_L\} .$$

Defining the ratio:

$$\text{Leading/Total} = \varrho_B$$

the four inclusive cross sections can be written as:

$$\varrho_B = \varrho_{\bar{B}} = (\text{Leading/Total}) ,$$
$$\varrho_M = \varrho_{\bar{M}} = \left[1 - (\text{Leading/Total})\right] .$$

At ISR, in each hemisphere, the ratio (Leading/Total) is $\sim 1/16$ for strangeness and $\sim 1/8$ for "charm". In our discussion we will study the behaviour of A^o as a function of (Leading/Total).

2.4.5. - The lepton decay distributions.

The data from CLEO[56] show that in the semileptonic decay of "beauty" mesons, M_b, the magnitude of the mass recoiling with respect to the leptons is very near to the D mass:

$$M_b \rightarrow Xe\nu , \quad \text{with} \quad M_X \sim M_D \approx 2.0 \text{ GeV}/c^2 .$$

Moreover, the mean charged multiplicity of the decay is 3.5, where the D contributes with 2.5 charged particles on average. We can conclude that, even at values of the mass as high as the mass of the M_b, the semileptonic decay proceeds via a 3-body decay. On the contrary, the mean charged multiplicity in the hadronic decays of the M_b mesons is 6.3, i.e. the hadronic decay of the M_b produces, on average, one D plus four charged particles plus two neutral particles:

$$M_b \rightarrow D + 6\text{-bodies}.$$

In the following we will consider two possibilities:

i) the total multiplicity of all decays is 3: this is the worst case for the Asymmetry A^o;

ii) the total multiplicity of all semileptonic decay is 3 and the decay is $K_{\ell 3}$-like for mesons and phase-space for baryons, while the total multiplicity of all the hadronic decays have the known values for "charm" and "beauty" (~ 3 for "charm", $\sim$ charm + 6 for "beauty"), and, for "top" and "superbeauty", the same multiplicity as "beauty". It should be noted that this is already a conservative hypothesis, since the hadronic decays of "top" and "superbeauty" can be expected to produce more particles than "beauty". Higher values of multiplicity would produce higher values for the asymmetry.

2. 4. 6. - Estimates of the Asymmetry A^o.

In order to estimate the Asymmetry A^o, we have restricted our study to the case of electrons and positrons.

The detection acceptances ε have been evaluated by means of a Monte Carlo simulation, with the conditions set in the previous section and for 5 values of θ_{cut} ($\theta_{cut} = 10^o$, 20^o, 30^o, 40^o and 90^o).

Figures from 16a to 16t show the e^- acceptances for $\theta_{cut} = 30^o$ and model (ii) of section 2. 4. 5 for baryons, mesons and antimesons. The acceptances for e^+ originated by the decay of antibaryons are, of course, negligible.

Fig. 17 shows the behaviour of A^o (p_T, 30^o), for (Leading/Total) = = 0. 25 and model (ii) of section 2. 4. 5. There are two main peaks, one positive around $p_T = 10$ GeV/c, due to the "top" baryon decay into e^+, and one negative around $p_T = 19$ GeV/c, due to "superbeauty" baryon decay into e^-.

It is interesting to note that the separation between the two peaks depends only on the mass differences in the semileptonic decays of "superbeauty" and "top" states.

In fact in the 3-body semileptonic decay the transverse momentum spectrum of the electrons or positrons scales with $p_T/\Delta m$ where Δm is the difference between the parent mass and the mass of the hadronic particle produced in the decay. This is shown in Fig. 18 where the normalized $p_T/\Delta m$ spectra of the electrons and positrons produced in the decays:

i) $\Lambda^o_{sb} \rightarrow \Lambda^+_t e^- \bar{\nu}$;

ii) $\Lambda^+_t \rightarrow \Lambda^o_b e^+ \nu$;

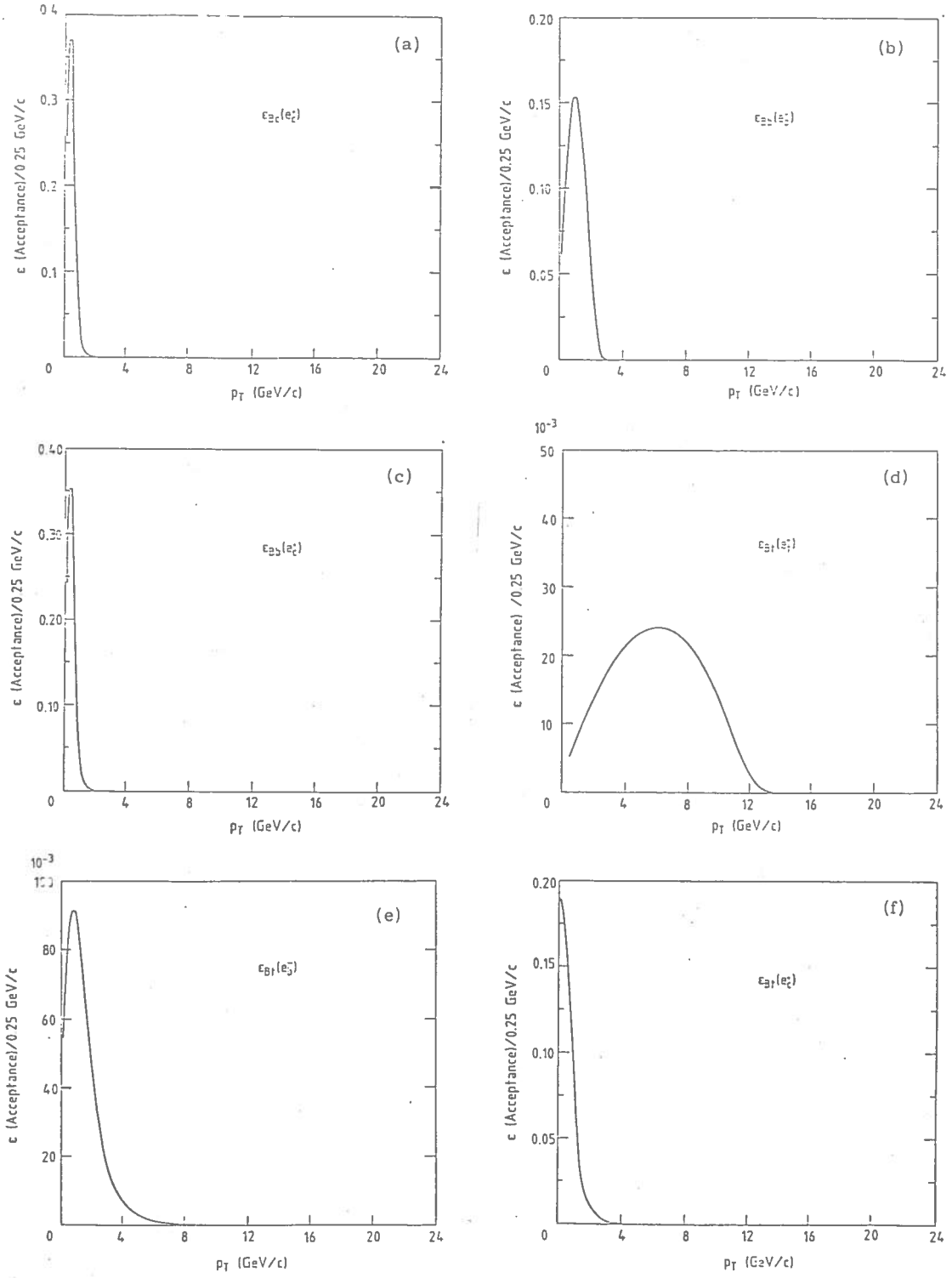

Fig. 16. (a) to (f): Acceptances ε for the various states and decay chains.

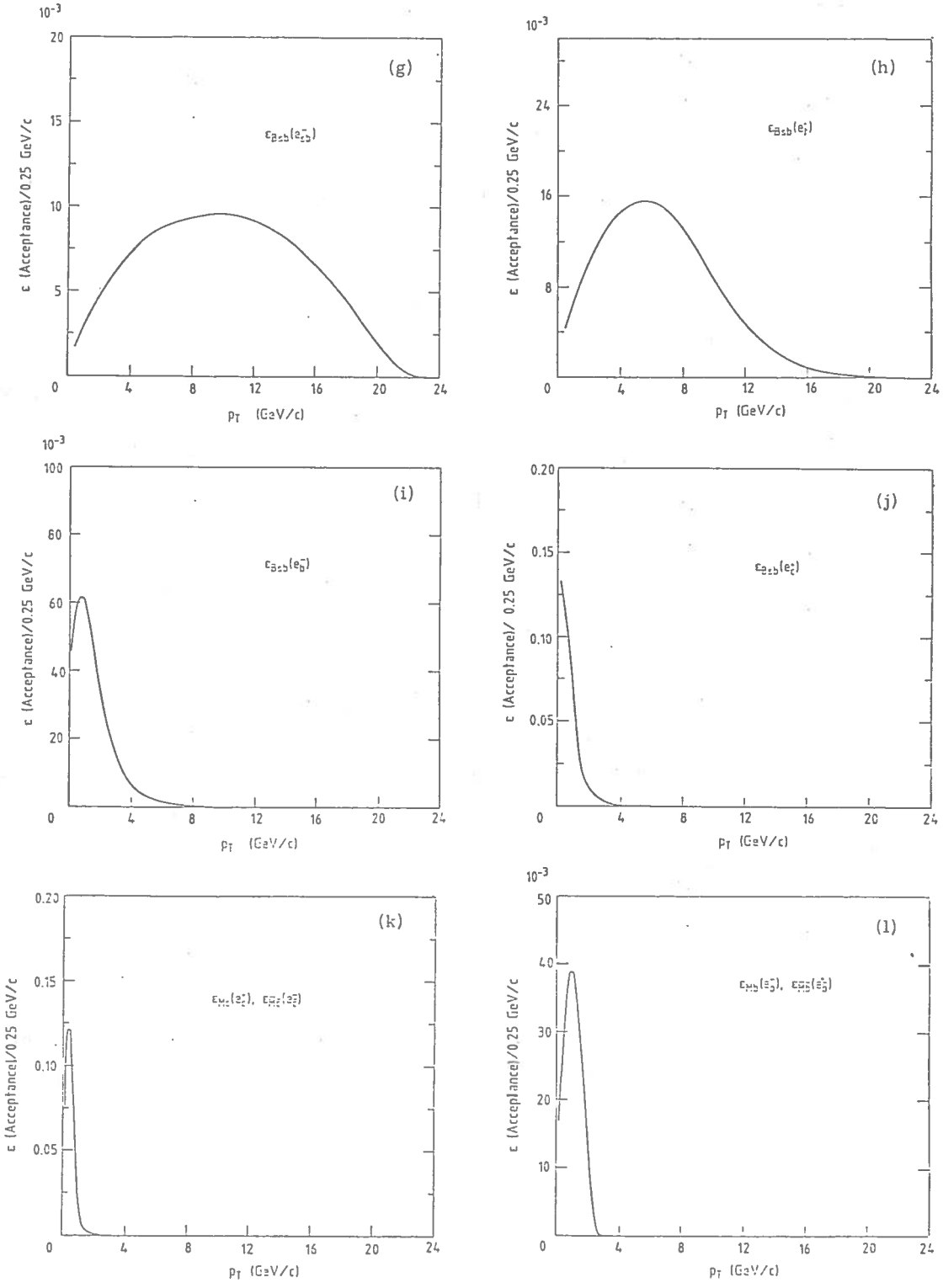

Fig. 16. (g) to (l): Acceptances ε for the various states and decay chains.

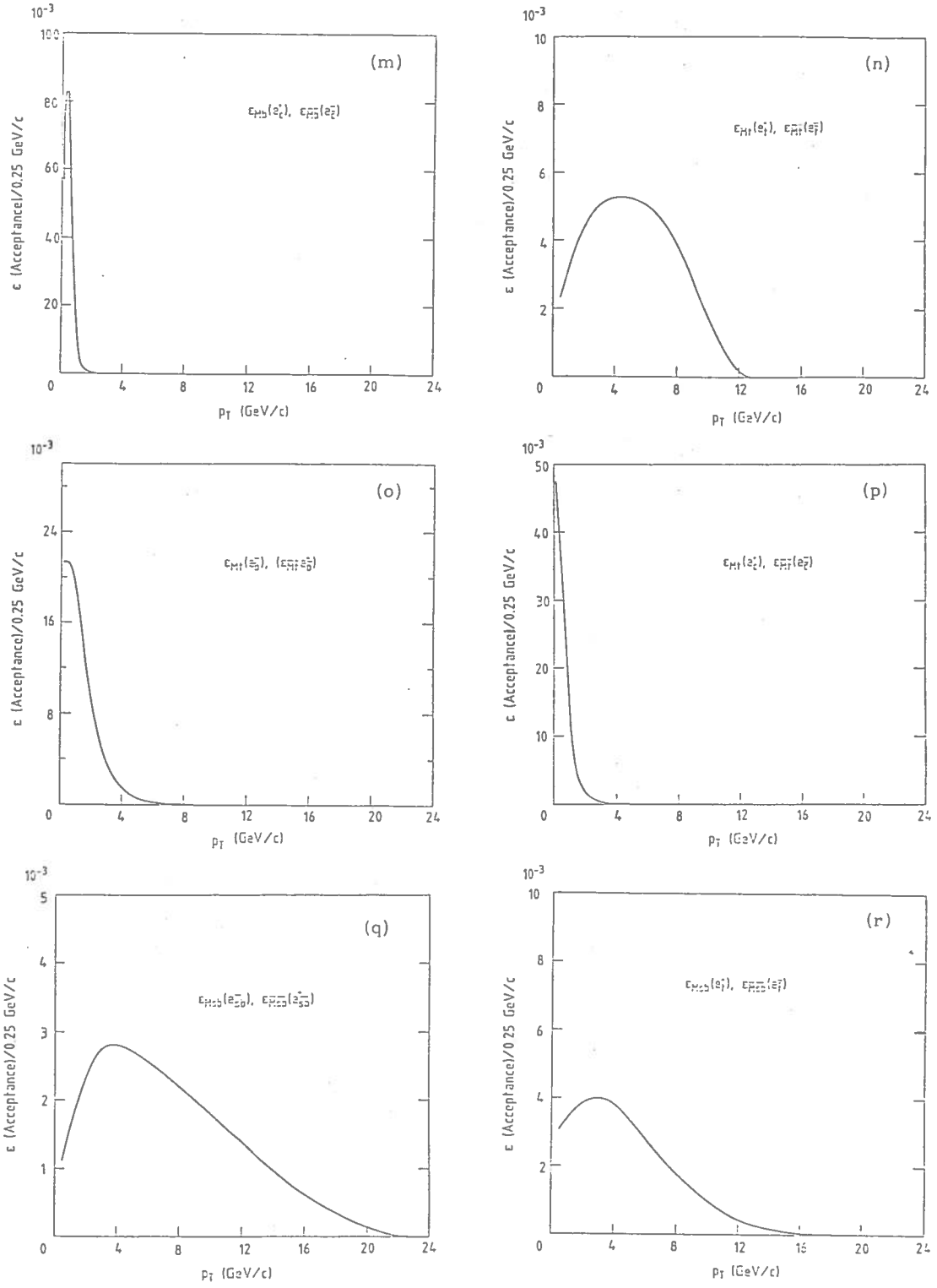

Fig. 16. (m) to (r): Acceptances ε for the various states and decay chains.

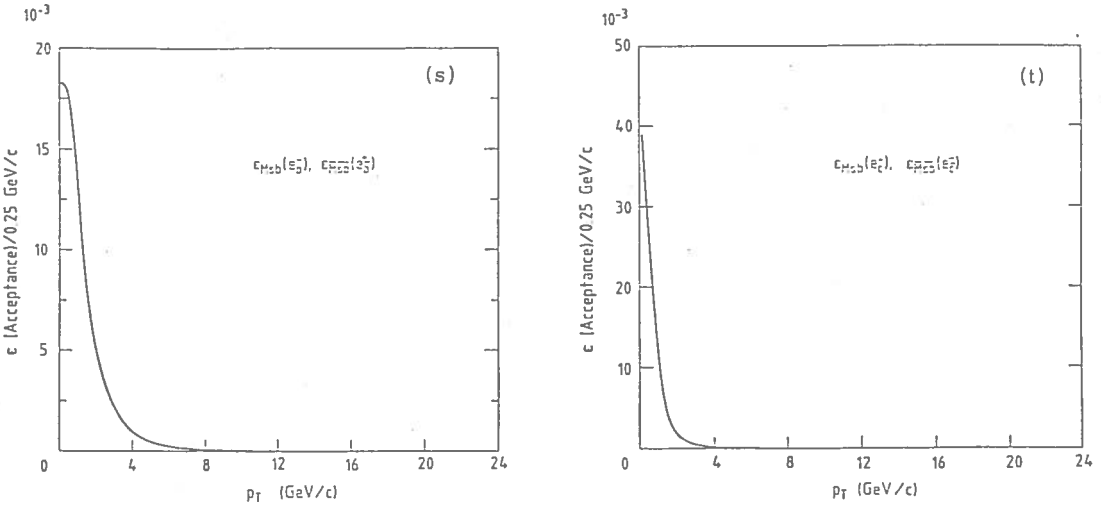

Fig. 16. (s) to (t): Acceptances ε for the various states and decay chains.

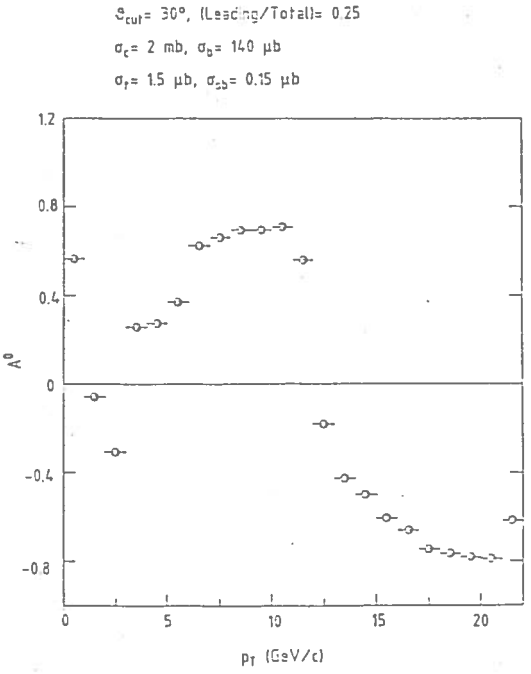

Fig. 17. Plot of $A^{o}(p_T, \theta_{cut} = 30^{o})$ as a function of p_T. The values assumed for the cross sections and for (Leading/Total) are indicated in the figure.

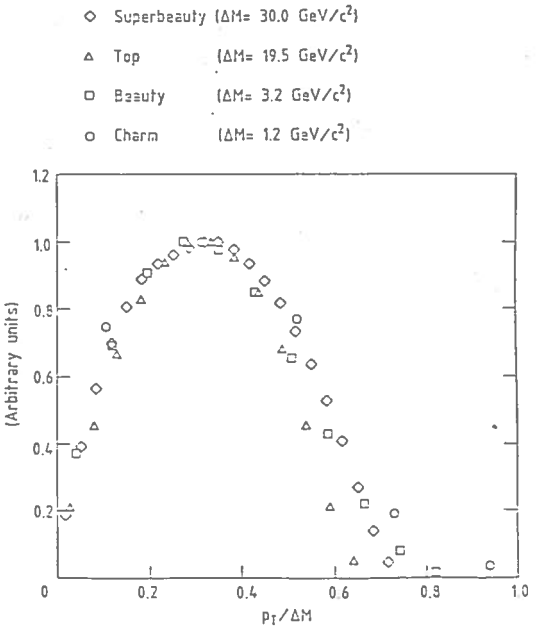

Fig. 18. Normalized $(p_T/\Delta m)$ spectra of the electrons from the decays: $\Lambda^{o}_{sb} \rightarrow \Lambda^{+}_{t} e^{-} \bar{\nu}$; $\Lambda^{+}_{t} \rightarrow \Lambda^{o}_{b} e^{+} \nu$; $\Lambda^{o}_{b} \rightarrow \Lambda^{+}_{c} e^{-} \bar{\nu}$; $\Lambda^{+}_{c} \rightarrow \Lambda^{o}_{s} e^{+} \nu$. The Δm values relative to the four decays are indicated in the figure.

iii) $\Lambda_b^o \rightarrow \Lambda_c^+ e^- \bar{\nu}$;

iv) $\Lambda_c^+ \rightarrow \Lambda_s^o e^+ \nu$;

are reported.

The mass differences Δm have the following values :

i) $\Delta m = m(\Lambda_{sb}^o) - m(\Lambda_t^+) \approx 30$ GeV/c^2 for the "sb" baryon decay;

ii) $\Delta m = m(\Lambda_t^+) - m(\Lambda_b^o) \approx 19.5$ GeV/c^2 for the "t" baryon decay;

iii) $\Delta m = m(\Lambda_b^o) - m(\Lambda_c^+) \approx 3.2$ GeV/c^2 for the "b" baryon decay;

iv) $\Delta m = m(\Lambda_c^+) - m(\Lambda_s^o) \approx 1.2$ GeV/c^2 for the "c" baryon decay.

Figs. 19a,b and 20a,b show the amplitude of the two peaks as a function of θ_{cut} and (Leading/Total) for : a) model (i) of section 2.4.5 (all 3-body decays) and : b) model (ii) of section 2.4.5 (greater multiplicity for the hadronic decays).

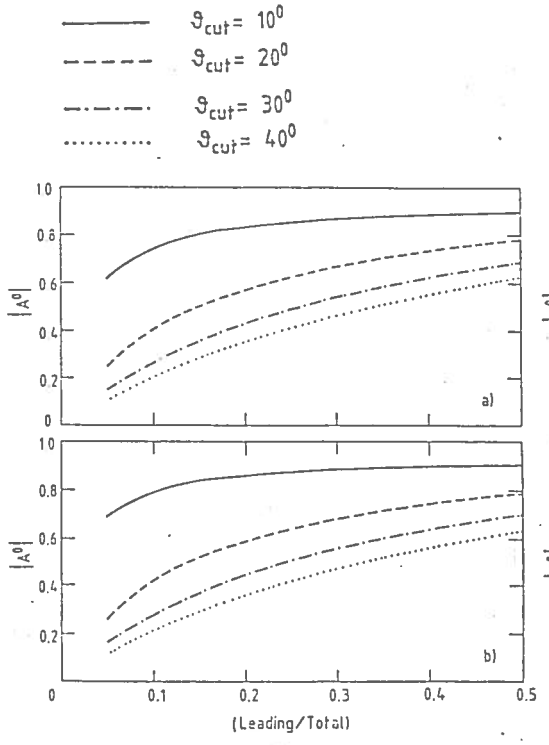

Fig. 19. Plot of $A^o(p_T = 10 GeV/c, \theta_{cut})$ ("top" peak) as a function of (Leading/Total) for different values of θ_{cut}, and using : a) model (i) of sect. 2.4.5, and b) model (ii) of sect. 2.4.5.

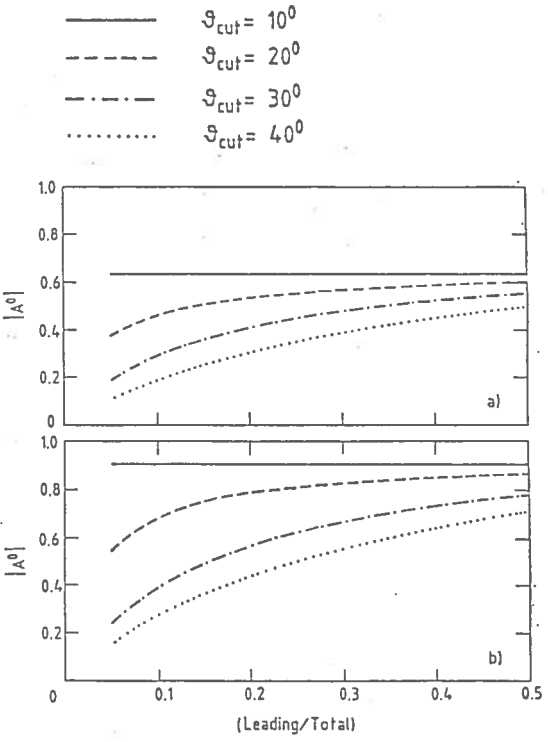

Fig. 20. Plot of $A^o(p_T = 19 GeV/c, \theta_{cut})$ ("superbeauty" peak) as a function of (Leading/Total) for different values of θ_{cut}, and using : a) model (i) of sect. 2.4.5, and b) model (ii) of sect. 2.4.5.

2. 4. 7. - Background evaluation.

In what has been described so far, the background contamination in the sample of prompt e^+ and e^- has not been considered. It is mainly due to:

i) the misidentification of charged and neutral hadrons in the experimental apparatus;
ii) the prompt e^+ or e^- production from sources other than open heavy flavour states.

The contribution (i) can be derived by extrapolating, above $p_T \simeq 10$ GeV/c the inclusive pion cross section as measured by the UA1 experiment[64], using the fit to their data:

$$E(d^3\sigma/dp^3) = A \times p_o^n/(p_o + p_T)^n \qquad (7)$$

with $A = 0.46 \pm 0.10\ mb^2\, c^2\, GeV^{-2}$, $p_o = 1.3 \pm 0.18\ GeV\, c^{-1}$ and $n = 9.14 \pm \pm 0.77$.

Formula (7) is relative only to charged pions (averaged over the two charges) and is given in unit of rapidity. We have assumed the contribution to the background due to the neutral pions to ~ 0.2 of the cross section (7). The rapidity interval over which we integrated the background depends on the θ_{cut}:

$$\theta_{cut} = 90^o \Rightarrow \Delta y \approx 4.0\,,$$
$$\theta_{cut} = 40^o \Rightarrow \Delta y \approx 3.0\,,$$
$$\theta_{cut} = 30^o \Rightarrow \Delta y \approx 2.7\,,$$
$$\theta_{cut} = 20^o \Rightarrow \Delta y \approx 2.3\,,$$
$$\theta_{cut} = 10^o \Rightarrow \Delta y \quad 1.5\,.$$

The extrapolated background rates should be multiplied by a reduction factor representing the rejection of the background from source (i) in the experimental apparatus.

Concerning the prompt electron background (ii), we assume, as a first approximation, that it would be negligible when compared with the contribution (i).

2. 4. 8. - Estimate of the Asymmetry parameter inclusive of background.

Due to the background sources described in the previous section, the experimental Asymmetry parameter is given by:

$$A^{exp}(p_T, \theta_{cut}) = \frac{\left[N(e^+) + N_{bg}(e^+)\right] - \left[N(e^-) + N_{bg}(e^-)\right]}{\left[N(e^+) + N_{bg}(e^+)\right] + \left[N(e^-) + N_{bg}(e^-)\right]}$$

where $N_{bg}(e^{\pm})$ is the number of background positrons or electrons. A^{exp} can then be expressed as a function of A^o and of the Signal-to--Background ratio defined as:

$$\frac{\text{Signal}}{\text{Background}} \equiv \frac{N(e^{\pm})}{N_{bg}(e^{\pm})}$$

by assuming $N_{bg}(e^+) = N_{bg}(e^-) = N_{bg}(e)$ and by substituting, in turns, in the above equation of A^{exp}, the expression of $N(e^-)$ and $N(e^+)$ derived from the definition of A^o. The result is:

$$A^{exp} = \frac{A^o}{1 + \dfrac{1 + A^o}{N(e^+)/N_{bg}(e)}}, \quad \text{for } A^o > 0;$$

$$A^{exp} = \frac{A^o}{1 + \dfrac{1 - A^o}{N(e^-)/N_{bg}(e)}}, \quad \text{for } A^o < 0.$$

Fig. 21 shows the quantity A^{exp} plotted as a function of the Signal/Background ratio for various values of A^o. The results can be expressed with curves of constant A^{exp} as function of (rejection power) versus (cross section for "top" and "superbeauty" production), for different θ_{cut}, (Leading/Total) and decay models (Figs. 22 to 31).

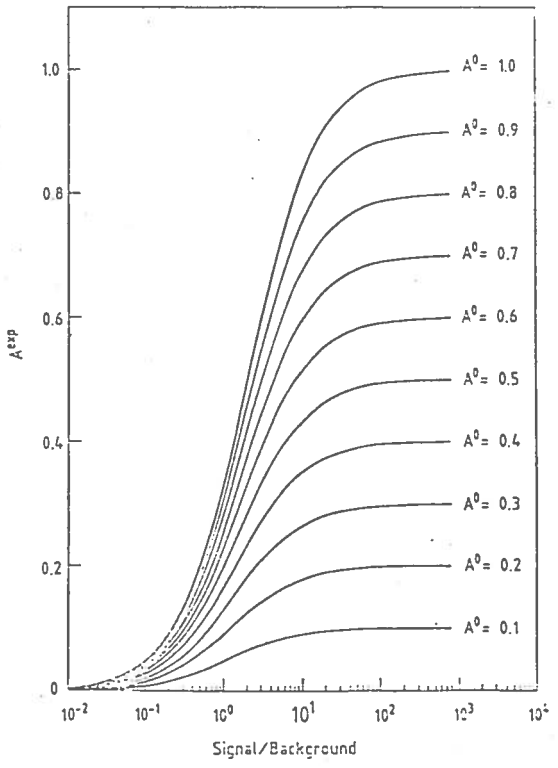

Fig. 21. The curves give the behaviour of A^{exp} as a function of Signal/Background, for different values of A^o.

The Table VI summarizes the results given in Figs. 22 to 31, for two values of the total cross section. They show the rejection powers needed to obtain $A^{exp} > 0.3$ or $A^{exp} < -0.3$, i. e. a reasonably high value for the Asymmetry, at the "top" and "superbeauty" peaks respectively. It can be seen that, with a rejection power of the order of 10^{-3}, a large range of θ_{cut}, (Leading/Total) and cross section values are accessible.

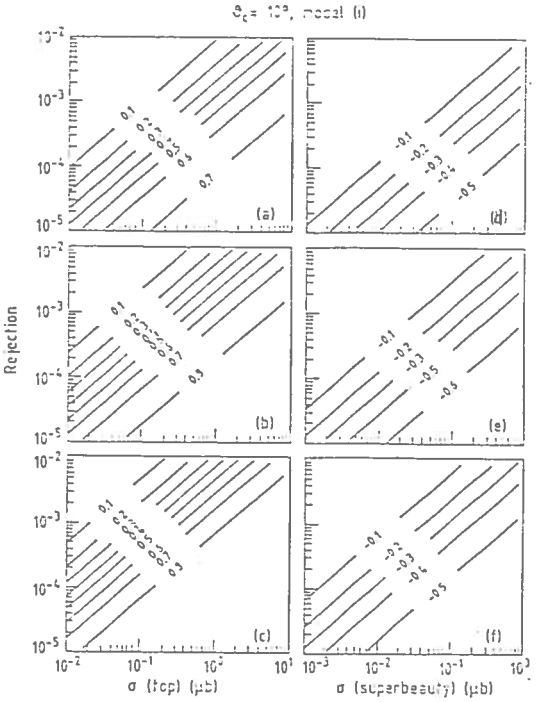

Fig. 22 - Curves of constant A^{exp}, in the plot (rejection power) versus (cross section for "top" or "superbeauty") for $\theta_{cut} = 10^{o}$ and for model (i). Plots (a), (b) and (c) refers to $p_T = 10$ GeV/c ("top" peak), plots (d), (e) and (f) refers to $p_T = 19$ GeV/c ("superbeauty" peak). Plots (a) and (d) are obtained with (Leading/Total) = 0.1, plots (b) and (e) with (Leading/Total) = 0.25, plots (c) and (f) with (Leading/Total) = = 0.5.

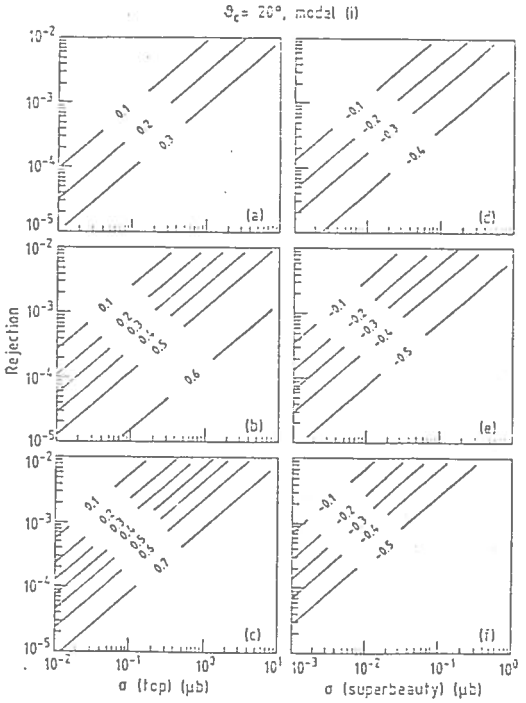

Fig. 23 - As Fig. 22 but for $\theta_{cut} = 20^{o}$ and model (i).

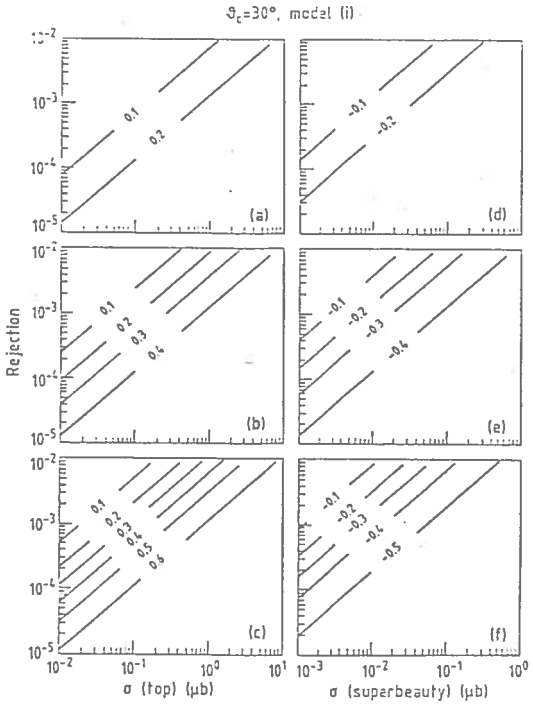

Fig. 24. As Fig. 22 but for θ_{cut} = = 30° and model (i).

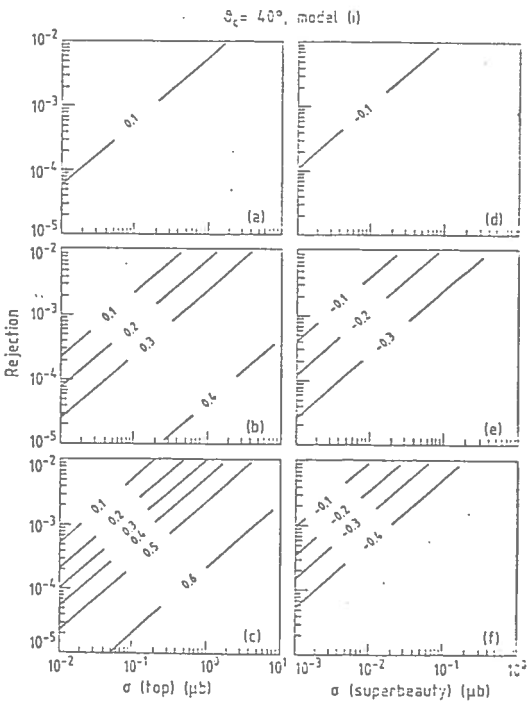

Fig. 25. As Fig. 22 but for θ_{cut} = = 40° and model (i).

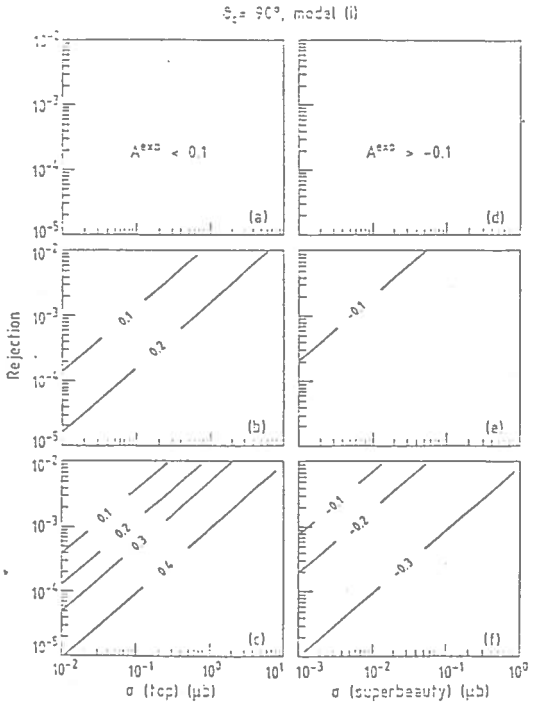

Fig. 26. As Fig. 22 but for θ_{cut} = = 90° and model (i).

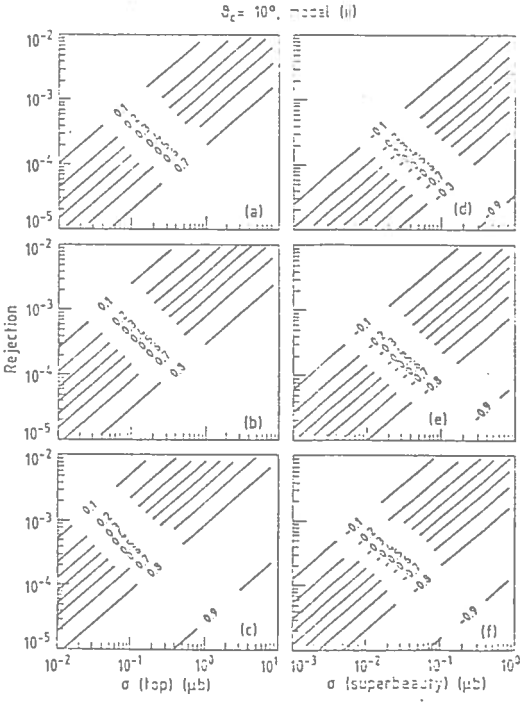

Fig. 27. As Fig. 22 but for θ_{cut} = = 10° and model (ii).

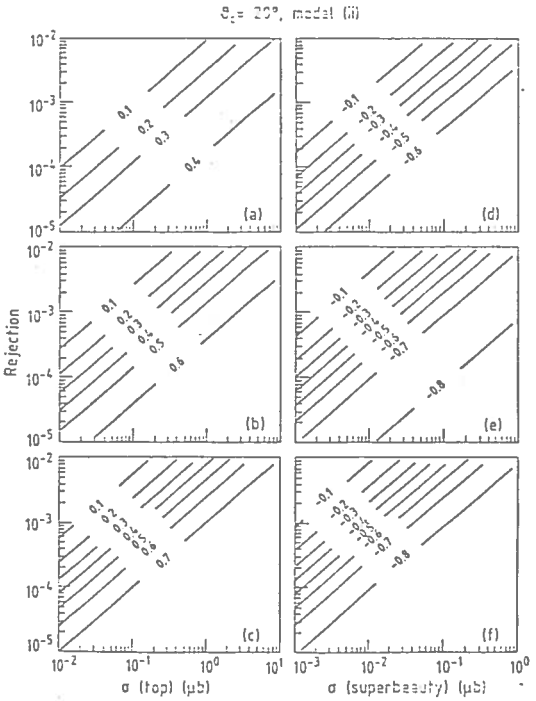

Fig. 28. As Fig. 22 but for θ_{cut} = = 20° and model (ii).

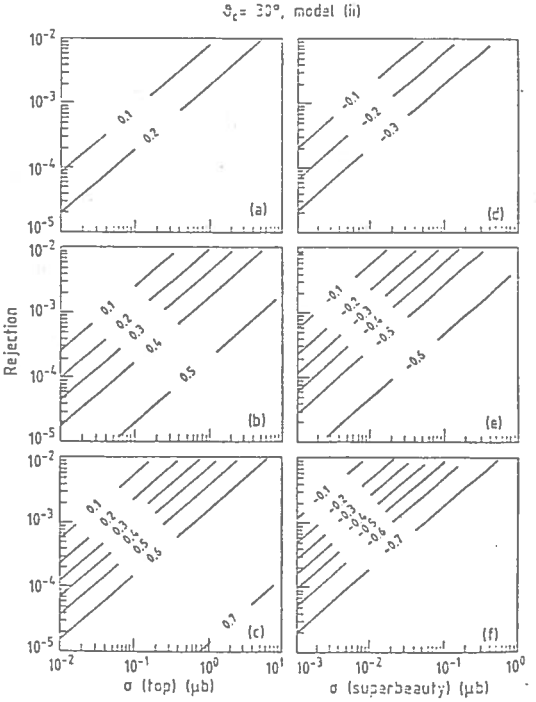

Fig. 29. As Fig. 22 but for θ_{cut} = = 30° and model (ii).

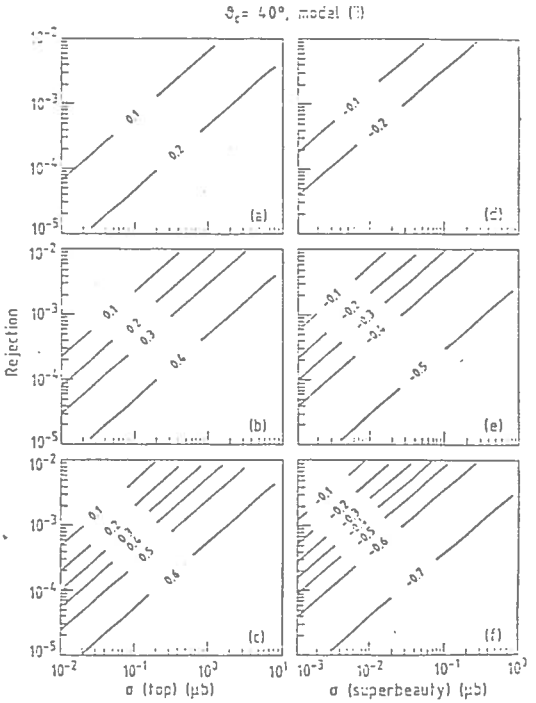

Fig. 30. As Fig. 22 but for θ_{cut} = = 40° and model (ii).

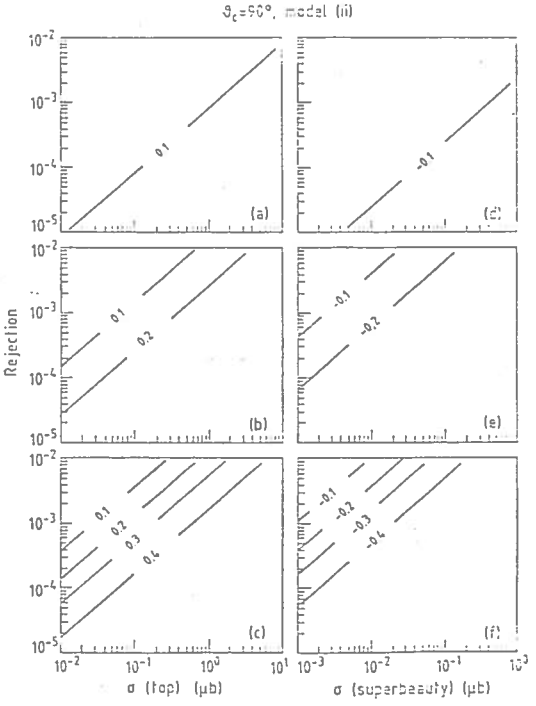

Fig. 31. As Fig. 22 but for θ_{cut} = = 90° and model (ii).

Table VI

θ_{cut}	(Leading/ /Total)	Cross section estimates			
		$\sigma_t = 1.5\ \mu b$, $\sigma_{sb} = 0.15\ \mu b$ (formula (9))		$\sigma_t = 0.1\ \mu b$, $\sigma_{sb} = 0.01\ \mu b$ (perturbative QCD)	
		model (i)	model (ii)	(model (i)	model (ii)
	P_T = 10 GeV/c				
10°	0.1	3.0	3.5	0.2	0.3
	0.25	10.0	12.0	0.6	0.7
	0.5	15.0	18.0	1.0	1.3
20°	0.1	1.3	1.5	0.1	0.1
	0.25	8.0	9.0	0.5	0.6
	0.5	20.0	23.0	1.0	1.2
30°	0.1	---	---	---	---
	0.25	6.0	7.0	0.4	0.4
	0.5	19.0	22.0	1.0	1.2
40°	0.1	---	---	---	---
	0.25	3.5	4.8	0.3	0.3
	0.5	17.0	21.0	1.0	1.1
	P_T = 19 GeV/c				
10°	0.1	0.4	1.0	0.02	0.1
	0.25	0.9	2.5	0.1	0.2
	0.5	1.7	4.5	0.1	0.3
20°	0.1	2.5	5.5	0.2	0.4
	0.25	10.0	20.0	0.5	1.0
	0.5	25.0	50.0	1.3	2.2
30°	0.1	---	2.2	---	0.2
	0.25	9.0	25.0	0.6	1.1
	0.5	23.0	45.0	1.6	2.0
40°	0.1	---	---	---	---
	0.25	4.0	19.0	0.3	1.0
	0.5	20.0	40.0	1.5	2.0

Rejection power in units of 10^{-3}.

2.4.9. - A detailed case.

As an example of what can be obtained experimentally in terms of the Asymmetry A^{exp}, let us fix in a reasonable way some of the parameters. We take (as in Figs. 29b and 29e):

i) (Leading/Total) = 0.25;
ii) $\theta_{cut} = 30^{o}$;
iii) decay model (ii).

Moreover, in order to have an estimate for the experimental errors on A^{exp}, we assume a total integrated luminosity $L = 300\ nb^{-1}$ (foreseen for 1983 at the CERN ($p\bar{p}$) Collider).

Figs. 32a and 32b show the plot of A^{exp} as a function of p_T, for a rejection power of 10^{-3} and for the two cross section estimates: as in section 2.4.1 (formula (6)) and as from perturbative QCD ($\sigma_t : \sigma_{sb} = 10:1$), respectively. The errors are purely statistic.

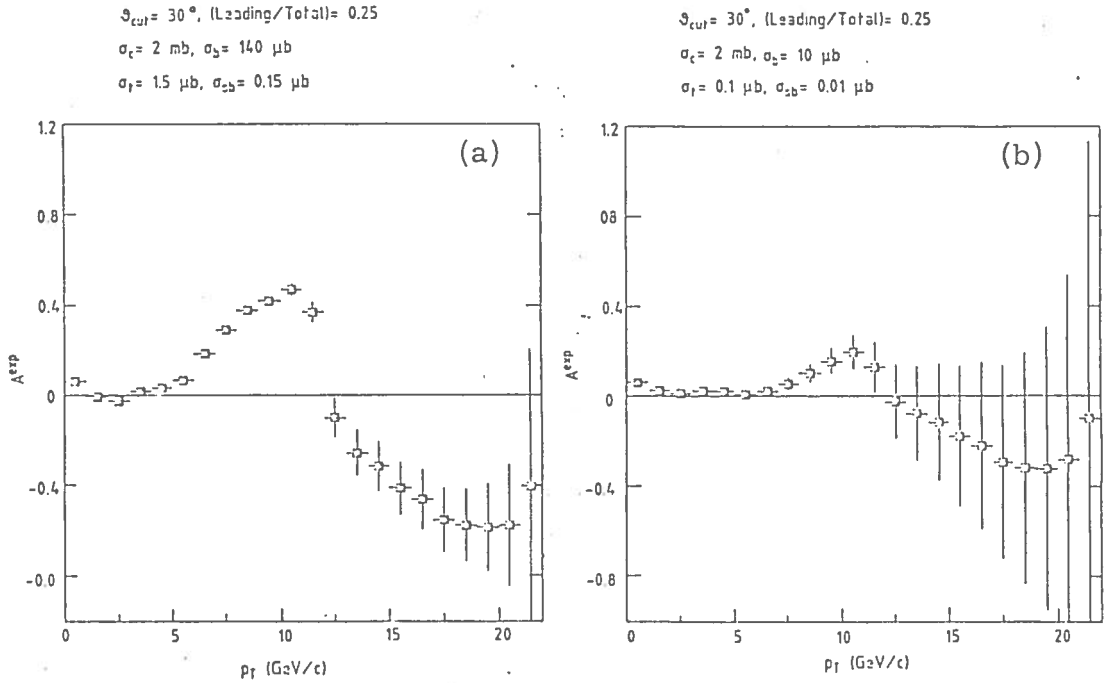

Fig. 32. Plot of A^{exp} as a function of p_T, for a total luminosity $L = 300\ nb^{-1}$, a rejection power of 10^{-3}, $\theta_{cut} = 30^{o}$ and (Leading/Total) = 0.25, using the cross section estimates. (a) from formula (6); (b) from perturbative QCD. The errors are statistical.

Figs. 33a and 33b show the expected number of produced electrons as a function of p_T, with the same two assumptions for the total cross sections. Superimposed is the expected background, as defined in section 2.4.7, and with a rejection factor of 10^{-3}.

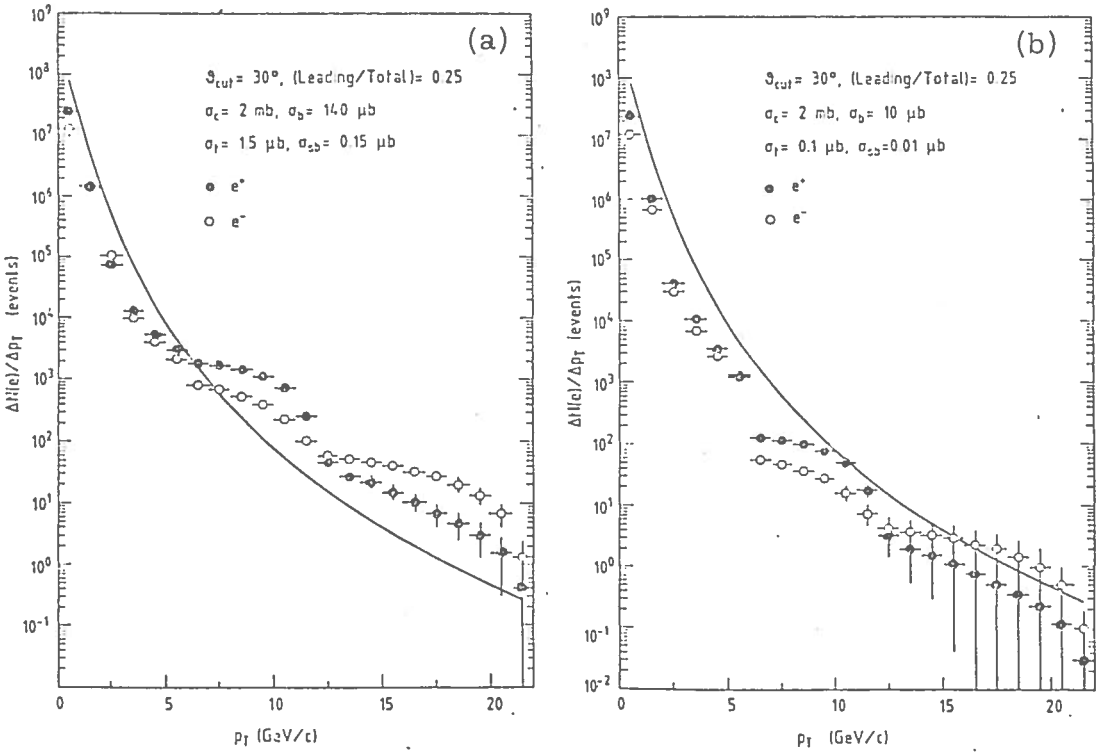

Fig. 33. Expected number of produced electrons as a function of p_T with the same assumptions as in Figs. 29b and 29e, and the two cross section estimates: (a) from formula (6); (b) from perturbative QCD. The errors are statistical.

It could be that the rejection factor needed is much less than 10^{-3}. In fact, a very heavy state (such as Λ_t^+ or Λ_{sb}^o) decaying semileptonically, may have the hadronic "jet" recoiling against the lepton pair. The study of the hadronic pattern associated with the (e^-) could be of such an help in the selection of good events, that a rejection power much below 10^{-3} could be sufficient. For example, an order of magnitude improvement would mean that the data which, at present, are quoted with a rejection of order 10^{-3} (Figs. 22-34), would reach the level of 10^{-4}. In this case, all our expectations would be scaled by this factor.

For completeness, let us mention that, at present, the (e/π) ratio in the p_T range above ~ 20 GeV/c is not known at the ($p\bar{p}$) Collider.

In order to compute the statistical significance of the observed effect, it is convenient to integrate A^{exp} over the p_T ranges:

i) $7 \leq p_T \leq 12$ GeV/c, corresponding to the "top" region;

ii) $14 \leq p_T \leq 23$ GeV/c, corresponding to the "superbeauty" region.

This is equivalent to the experimental procedure of fitting the data to reduce the statistical errors on the single points.

Figs. 34a and 34b show the number of standard deviations that can be obtained in the measurement of A^{exp}, respectively in the "top" and in the "superbeauty" regions, as function of the total cross sections σ_t and σ_{sb}, in the same conditions specified above. The 90% confidence

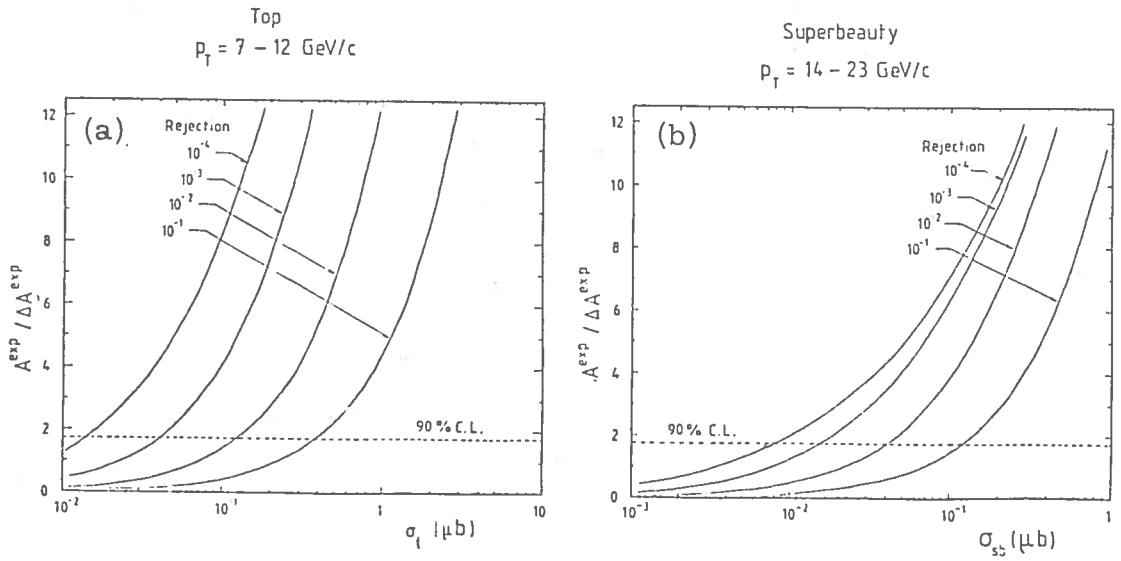

Fig. 34. The statistical significance of the measurement of A^{exp} ($A^{exp}/\Delta A^{exp}$), is shown, for a total luminosity of L = 300 nb^{-1}. $\theta_{cut} = 30^{o}$ and (Leading/Total) = 0.25, and for the two p_T ranges: (a) p_T = 7-12 GeV/c; (b) p_T = 14-23 GeV/c.

level in the measurement is also shown. These results show that, especially in the "top" case, a high statistical significance can be reached with a moderate rejection power, even if the total cross section for "top" production is as low as 0.1 μb, i. e. the value predicted by QCD.

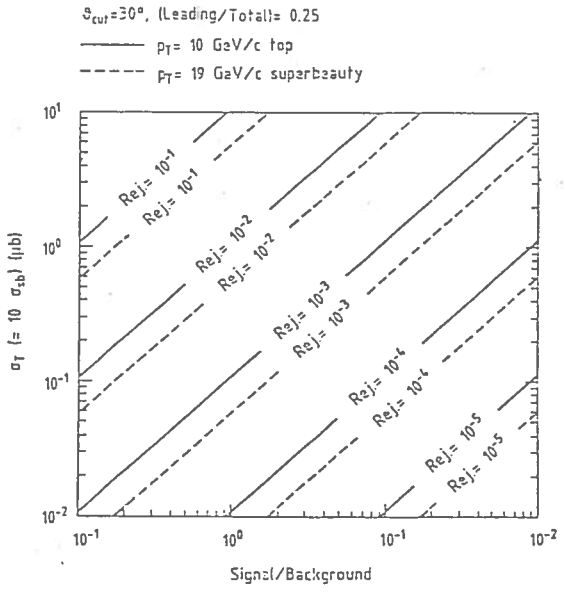

In Fig. 35, the behaviour of the ratio (Signal/Background) as a function of the total cross section for "top" and "superbeauty" and for different values of the rejection power, is shown.

Fig. 35. Correspondence between rejection power and signal-to-background ratio (Signal/Background) as function of total cross section for "top" and "superbeauty" production, and at the two p_T values: 10 GeV/c and 19 GeV/c.

2. 5. - Comparison with preliminary data from the CERN ($p\bar{p}$) Collider.

As a first step in the study of the heavy-quark physics using the ($p\bar{p}$) Collider, we propose to compare our predictions with the data already available from the ($p\bar{p}$) Collider.

In its search for electron candidates, the UA1 Collaboration finds 16 events with an isolated electron[58]. Five of these events are attributed to $W^{\pm}$ decay, whilst the remaining 11 are characterized by a "jet activity" in the azimuthal region opposite to the isolated electron. The events correspond to a total integrated luminosity of $L = 20\ nb^{-1}$.

According to the Monte Carlo discussed in detail in the previous section, the acceptance for electrons originating from "superbeauty" decays in the phase-space region defined by the UA1 data ($p_T > 15\,GeV/c$ and, for the polar angle, $25^{\circ} < \theta < 155^{\circ}$) is, for baryon and antibaryon decays,

$$\varepsilon_B(e^{\pm}) = 0.08 ,$$

and for meson and antimeson decays

$$\varepsilon_M(e^{\pm}) = 0.12 .$$

We can therefore use the approximation

$$\varepsilon(e^{\pm}) = \varepsilon_B(e^{\pm}) = \varepsilon_M(e^{\pm}) = 0.1 .$$

Since the heavy flavours are produced in pairs, the total efficiency for seeing at least one electron from the leptonic decay of "superbeauty" is

$$\varepsilon_T(e^{\pm}) = 2 \times \varepsilon(e^{\pm}) = 0.2 ,$$

where we have assumed equal semileptonic branching ratios for baryon and meson decays.

The request for "jet activity" opposite in azimuth to the electron, gives rise to another acceptance factor, $\varepsilon_T(\text{jet})$, which we can derive by analysing the hadronic pattern of the "superbeauty" semileptonic decays predicted by our Monte Carlo, according to the "jet" definition outlined by the UA1 Collaboration, i. e.

i) all particles with $p_T > 2.5$ GeV/c are associated with a jet if their separation in phase-space is

$$\Delta R = \sqrt{(\Delta\phi)^2 + (\Delta\eta)^2} < 1 ,$$

with $\Delta\phi$ in radians and η (= pseudorapidity) $= -\ln(\operatorname{tg}\theta/2)$;

ii) all other particles are associated with the jet defined as in point (i), if they satisfy the conditions

p_T relative to the jet < 1 GeV/c ,
θ relative to the jet $< 45^o$;

iii) the total transverse energy of the jet must be greater than 10 GeV.

The result is

$$\varepsilon_T(\text{jet}) \simeq 70\% .$$

On the other hand, as shown in Fig. 36, the condition that the jet is opposite in azimuth to the electron within $\Delta\phi = 30^o$ is nearly always satisfied.

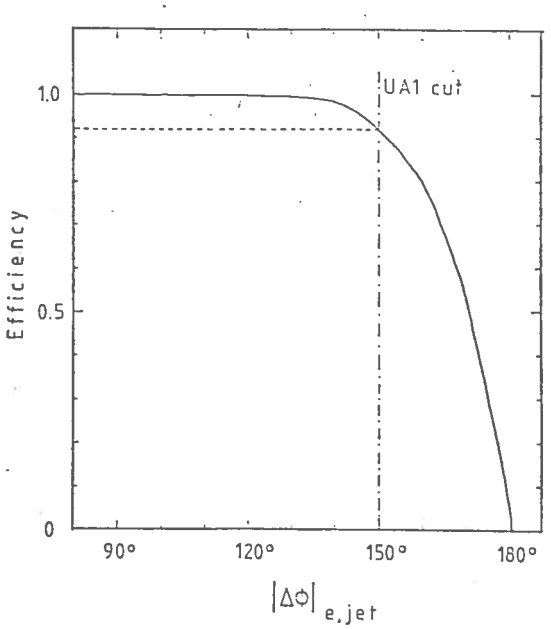

Fig. 36. Efficiency versus the cut value in the difference of azimuth $|\Delta\phi|$ between the electron and the hadronic jet in "superbeauty" decay, as derived from the Monte Carlo simulation.

The number of electrons from "superbeauty" semileptonic decays in the UA1 electron sample is therefore given by

$$N(e^{\pm}) = \sigma_{sb} \times BR \times L \times \varepsilon_T(e^{\pm}) \times \varepsilon_T(\text{jet}) , \qquad (8)$$

where BR is the semileptonic branching ratio of the "superbeauty" state, taken to be BR $\simeq 0.15$, and σ_{sb} is the cross section for the production of "superbeauty" particle states at the $(p\bar{p})$ Collider; the other symbols have already been defined. The UA1 results show that $N(e^{\pm}) = 11 \pm 3$.

Note that in Eq. (8) the efficiencies for the electron trigger have not been taken into account. They are as follows:

i) The efficiency for detecting "isolated" electrons, i. e. with no other particles with $p_T > 2$ GeV/c in a 20^o cone around the electron direction. Here the risk is in the random vetoing, otherwise the efficiency for genuine events is very high. From UA1 data[58] it is possible to deduce the upper limit for random vetoing: it must be below 75%, and it could, in fact, be almost zero.

ii) The efficiency of the energy cut $E_T > 15$ GeV/c owing to the finite

resolution of the electromagnetic shower detectors (EMSDs). This efficiency can be evaluated to be > 95%, using the quoted EMSDs energy resolution ($\Delta E/E = 0.15/\sqrt{E}$).

Figure 37a shows the cross-section corresponding to the (11 ± 3) events observed. Notice that the "experimental" finding of UA1 falls in a remarkable range of agreement with the crude extrapolation from "charm" and QCD.

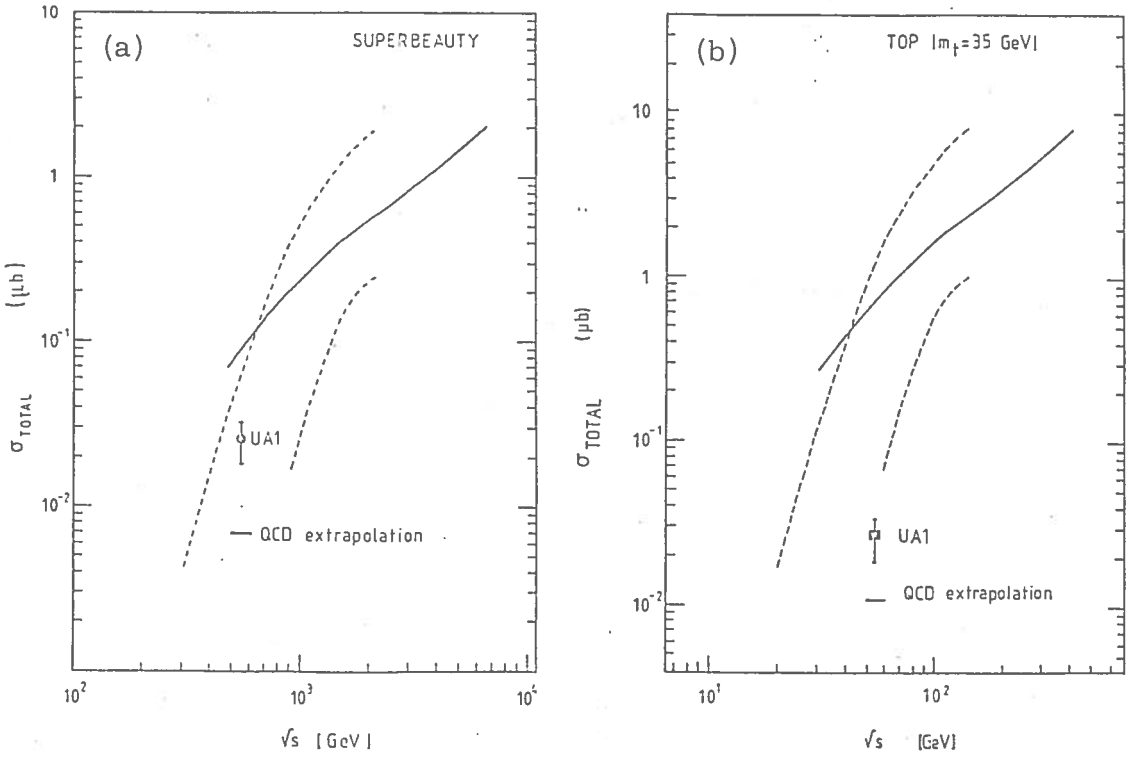

Fig. 37. Comparison between the UA1 results and the cross-sections for: (a) superbeauty ($m_{sb} = 55$ GeV/c^2); (b) top ($m_t = 35$ Gev/c^2); derived from strange (full line) and charm (dashed lines) cross-sections following formula (4).

Going further, we have compared the p_T distributions of the ($e^{\pm}$) from UA1 with that from our Monte Carlo simulation. This is shown in Fig. 38, where the Monte Carlo expectations are obtained using different values for the parameter b in the "superbeauty" production process

$$d\sigma/dp_T \propto p_T \exp(-bp_T).$$

Data and Monte Carlo distributions are normalized to the total number of events with $p_T > 15$ GeV/c.

A value of $b \simeq 0.20\ GeV^{-1}c$, i.e. a value for the production average transverse momentum $\langle p_T \rangle$ of the order of 10 GeV/c, fits the UA1 data quite well. This value for b is much smaller than the value (b = 2.5) which we found in our study of "charm" production at the ISR[4,16]. However, it should be noticed that here we are dealing with the production of a flavour much heavier than "charm". The value b = 0.2 is in good agreement with the prescription $\langle p_T^2 \rangle \simeq m^2/4$ (m is the quark mass) used by Odorico[51] to compute the "charm" production properties from flavour excitation.

The efficiency for detecting electrons with $p_T > 15$ GeV/c in the Monte Carlo simulation does not change very much for b > 0.2, as shown in Fig. 39. Thus the total "superbeauty" cross-section derived by Eq. (8) holds, within ± 30%, even with this very low but expected value of b.

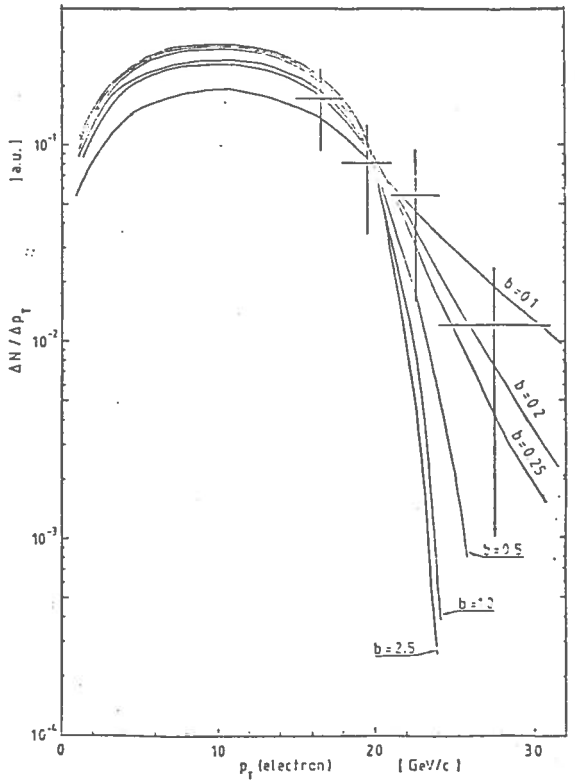

Fig. 38. p_T spectra of the electrons produced in the decay (sb) → teν, for different $(d\sigma/dp_T) \propto p_T \exp(-bp_T)$ production distributions of the parent (sb) particle, and comparison with UA1 data. The normalization is for $p_T > 15$ GeV/c.

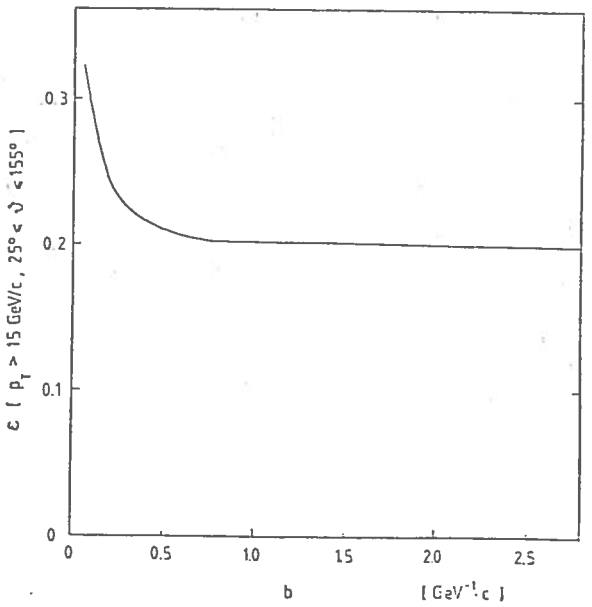

Fig. 39. Efficiency of the Monte Carlo simulation for the UA1 electron selection, as a function of the exponent parameter b in the parent (sb) p_T production distribution.

As mentioned above, the "down-like" nature of the observed (11 ± 3) events cannot be established in a direct way. It is based on a chain of self-consistent arguments. Let us give up the mass ratio (1) which binds the "top" flavour to be in the 25 GeV/c^2 range. If we repeat the analysis without this constraint, the (11 ± 3) events can be reinterpreted as the "up-like" signature with the "top" flavour mass 30 GeV/c^2 above the beauty flavour. The value of the cross-section would in this case be as shown in Fig. 37b.

A sequence of arguments based on known facts and on simple hypotheses, extrapolated to the CERN ($p\bar{p}$) Collider energies, allows us to conclude that the (11 ± 3) events observed by the UA1 Collaboration and consisting each of a single $(e^{\pm})$ accompanied by a jet activity in the opposite hemisphere, correspond to a value of the cross-section expected for the production of a very heavy flavoured state, in the 55 GeV/c^2 mass range. Moreover, the observed transverse momentum spectrum of the $(e^{\pm})$ follows the expectations for the semileptonic decay of a very massive state, again in the 55 GeV/c^2 mass range.

It should, however, be noticed that the identification of the "down-like" nature of the heavy-flavoured state is based on a series of hypotheses which produce the correct $\Delta m \simeq 30$ GeV/c^2 for the $(e^{\pm})$ transverse momentum spectrum, and the correct magnitude for the cross-section. If we were to ignore the cross-section and the quark mass ratios which allow us to predict the masses of the 4^{th} family, the only parameter left to fit the observed $(e^{\pm})$ transverse momentum spectrum would be the value $\Delta m \simeq 30$ GeV/c^2. In this case the conservative interpretation of the UA1 results would be a "top" with a mass 30 GeV/c^2 above the "beauty".

This shows the importance of our proposal to study in detail the production of new heavy flavours at the CERN ($p\bar{p}$) Collider by measuring the (e^+/e^-) asymmetry. In fact, the sign of the asymmetry allows the identification of the "up-like" or "down-like" nature of the heavy-flavoured state in a direct and unambiguous way. Moreover, the (e^+/e^-) energy dependence of the asymmetry enables us to establish the correct sequence of

"down-like" $\longleftrightarrow$ "up-like"

decay chains for the new heavy flavours, and their mass difference.

2.6. - Conclusions.

The following conclusions are in order:

i) Past experience says: do not take too seriously the "theoretical" QCD predictions; many things still do not fit between theory and experiments. In particular, neither the large "charm" cross sec

tions, nor the "Leading" effect were predicted.

ii) A detailed study of the production mechanism of heavy flavours at the ISR is important in order to make reasonable extrapolations to the ($p\bar{p}$) Collider energy.

iii) The number of "new" states with heavy flavours is very large. If their production cross sections follow the simple extrapolation proposed by us, the CERN ($p\bar{p}$) Collider would be a quasi-factory for these new states. The problem is to have the instrumentation able to detect their existence.

iv) The study of the electron-positron asymmetry and of its energy dependence is of the utmost importance at the ($p\bar{p}$) Collider. If the "Leading" effect follows the same trend as "charm" at the ISR, this asymmetry is expected to be detectable, even if the production cross sections of the heavy flavoured states would follow the QCD predictions.

The study of the electron asymmetry and of its energy dependence is not less important then the searches for the Z^o and the $W^{\pm}$. Finding the Z^o and the $W^{\pm}$ tell us nothing about one of the most crucial problems of Subnuclear Physics: the families problem.

A detailed study of the electron asymmetry allows to investigate the presence, in a mass range so far unaccessible to any other machine, of the new flavours up-like ("top") and down-like ("superbeauty"), and to determine their mass relation.

3. - MULTIHADRONIC FINAL STATES

3.1. - Introduction and the "Leading" effect.

In a long series of systematic studies on the properties of multiparticle hadronic systems produced in low p_T (pp) interactions, at the ISR, we have discovered a remarkable set of analogies between the properties of the multiparticle systems produced in low p_T(pp) interactions, (e^+e^-) annihilation and in deep-inelastic scattering (DIS) processes[21-46].

These analogies are based on the following quantities:

1) the inclusive fractional energy distribution of the produced particles [21, 22, 30, 38] (see Figs. 40-42, 54);

2) the average charged particle multiplicities[23, 29, 39, 41, 43] (see Figs. 43, 52, 53);

3) the ratio of the average energy associated with the charged particles over the total energy available for particle production[27] (see Fig. 44);

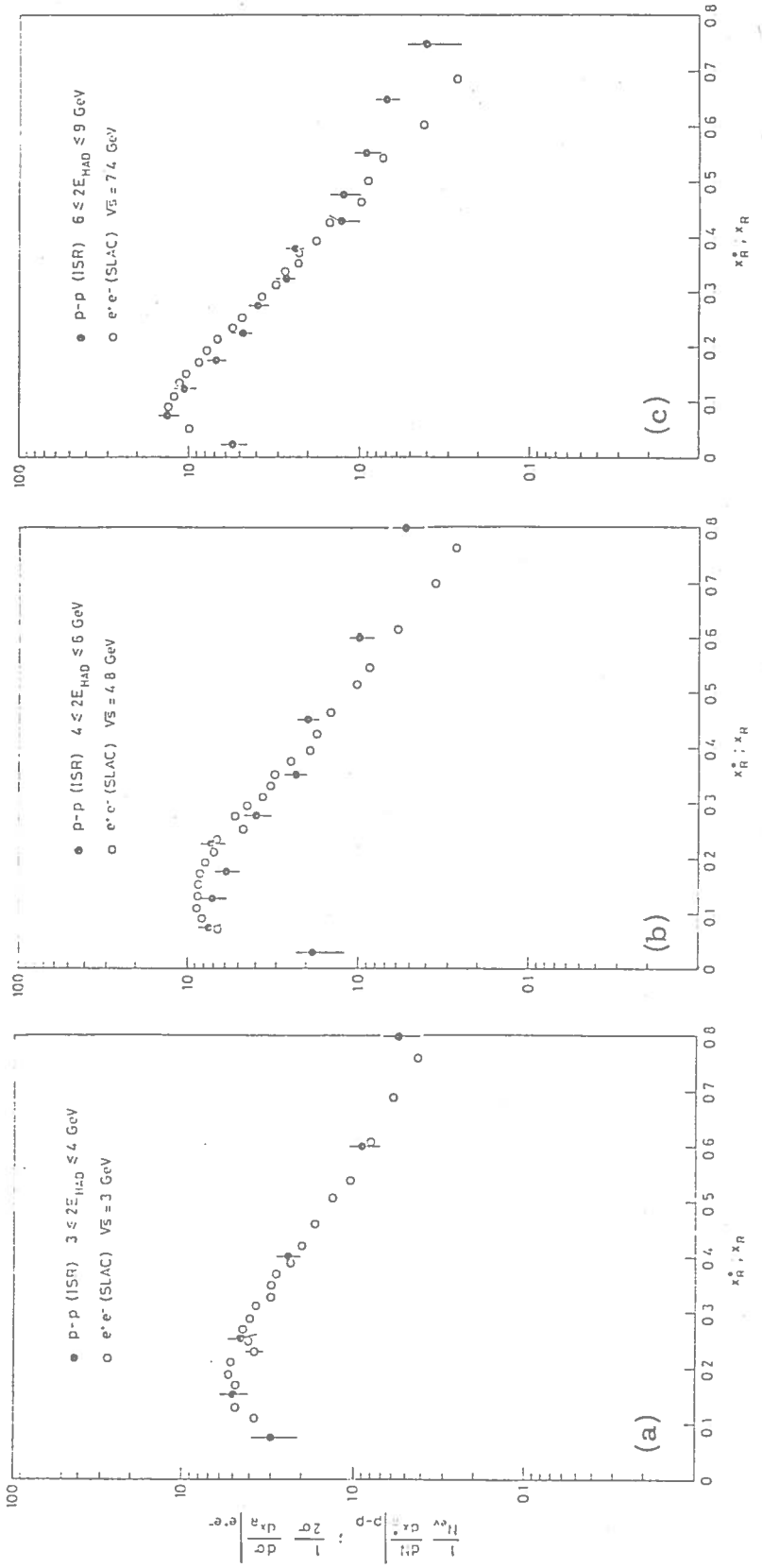

Fig. 40. The inclusive single-particle fractional momentum distributions $(1/N_{ev})(dN_{track}/dx_R^*)$ for data taken at $(\sqrt{s})_{pp} = 30$ GeV and for three intervals of $2E^{had}$: (a) $(3 \leq 2E^{had} \leq 4)$ GeV; (b) $(4 \leq 2E^{had} \leq 6)$ GeV; (c) $(6 \leq 2E^{had} \leq 9)$ GeV. Also shown are data from SPEAR at $(\sqrt{s})_{e^+e^-} = 3$, 4.8 and 7.4 GeV.

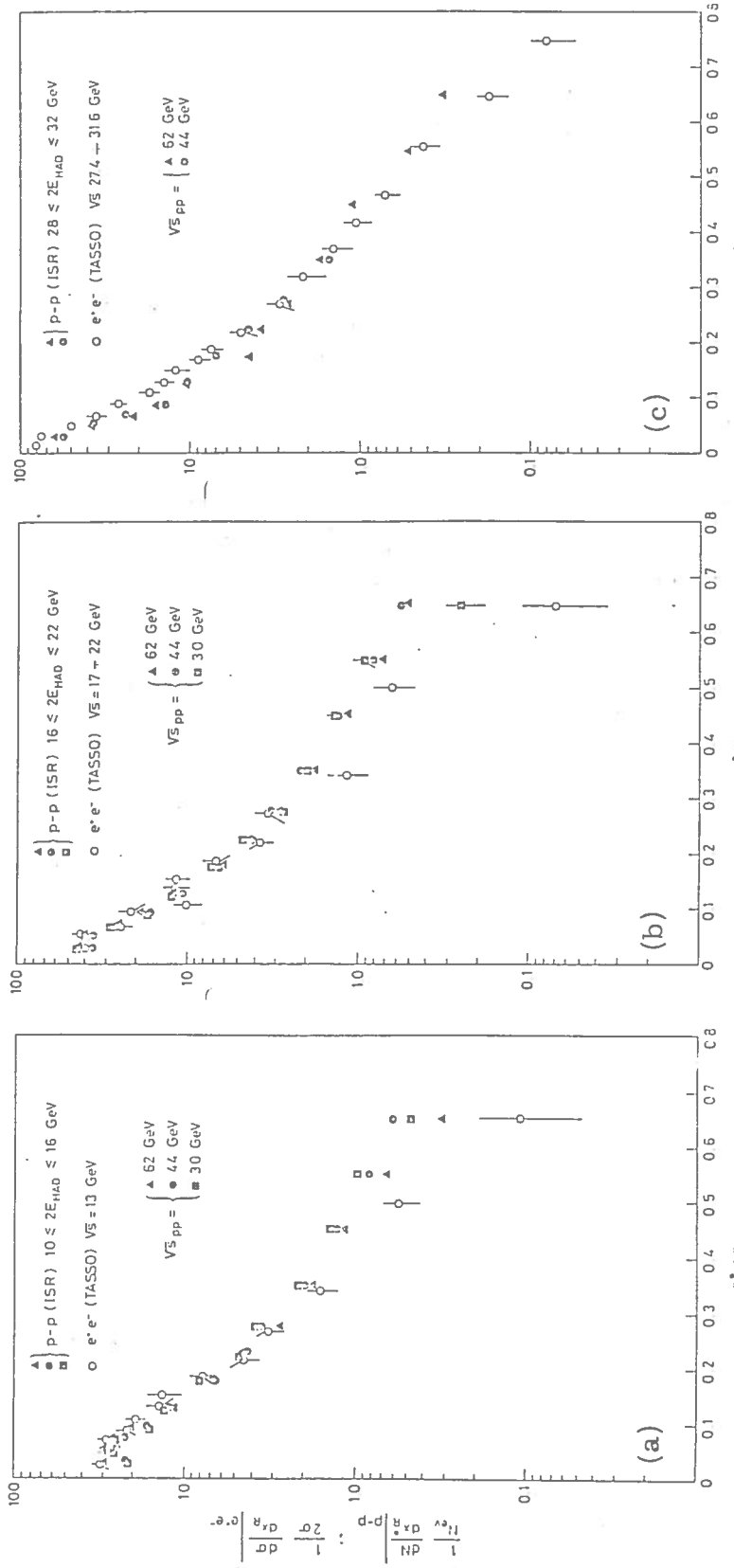

Fig. 41. The inclusive single particle fractional momentum distributions $(1/N_{ev})(dN_{track}/dx_R^*)$ for the following conditions:
(a) $(10 \leq 2E^{had} \leq 16)$ GeV, $(\sqrt{s})_{pp}$ = 30, 44 and 62 GeV; (b) $(16 \leq 2E^{had} \leq 22)$ GeV, $(\sqrt{s})_{pp}$ = 30, 44 and 62 GeV; (c) $(28 \leq 2E^{had} \leq 32)$ GeV, $(\sqrt{s})_{pp}$ = 44 and 62 GeV.
Also shown are data from TASSO at PETRA relative to $(\sqrt{s})_{e^+e^-}$ = 13, 17-22, and 27.4-31.6 GeV.

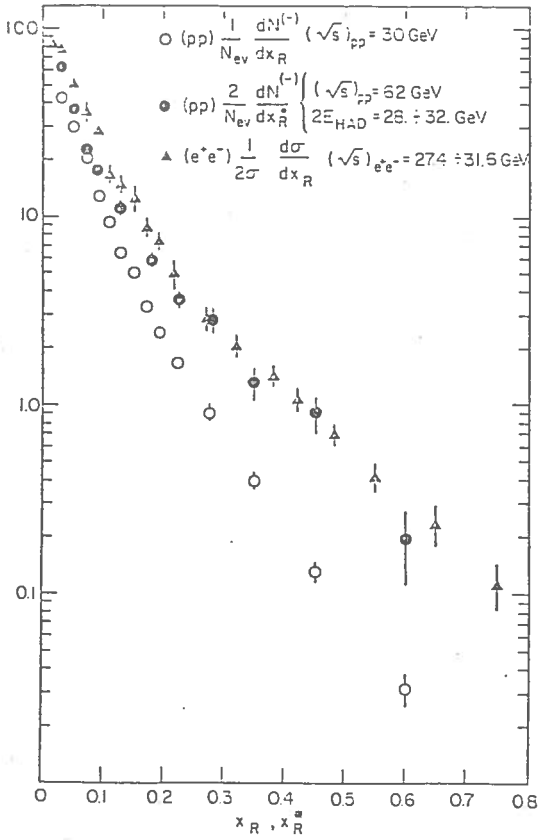

Fig. 42. The inclusive fractional momentum distributions of negative particles for (pp) interactions using the standard analysis at $(\sqrt{s})_{pp}$ = 30 GeV (white circles); using the method of removing the leading protons at $(\sqrt{s})_{pp}$ = 62 GeV and $2E^{had}$ = 28-32 GeV (black circles); the (e^+e^-) data at $(\sqrt{s})_{e^+e^-}$ = 27.4-31.6 GeV (black triangles).

4) the inclusive transverse momentum distribution of the produced particles[28, 33] (see Figs. 45-47);

5) the correlation functions in rapidity[42] (see Fig. 48).

The key point in these studies is the new method introduced in order to study (pp) interactions at the ISR. This method is based on the subtraction of the "Leading" protons effect from the final state of a (pp) interaction. Once this "Leading" protons are subtracted out, it is possible to work in the correct reference frame of the multiparticle system produced. Moreover, it is possible to calculate the "effective" energy available for particle production defined as

$$\sqrt{(q_{tot}^{had})^2} = \sqrt{(q_1^{inc} + q_2^{inc} - q_1^{Leading} - q_2^{Leading})^2} \qquad (9)$$

where $q_{1,2}^{inc}$ and $q_{1,2}^{Leading}$ are respectively the four vectors of the incident and "Leading" protons.

This "effective" energy can be very different from the "nominal" total energy of the ISR proton beams.

Let us point out that the "Leading" proton effect (see Fig. 49) is not a phenomenon limited to the ISR case; nor to the proton-proton

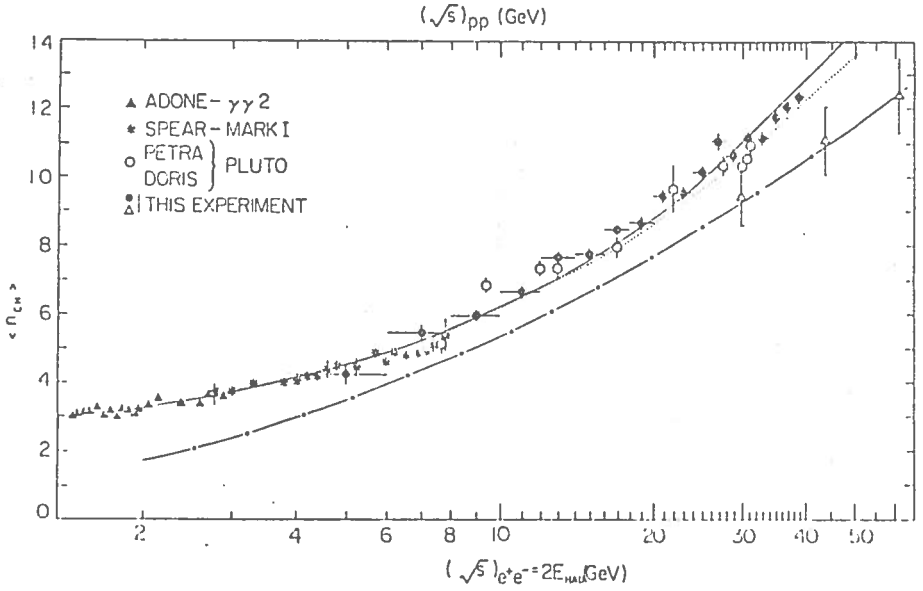

Fig. 43. Mean charged particle multiplicity, averaged over different $(\sqrt{s})_{pp}$, versus $2E^{had}$, compared with (e^+e^-) data. The contribution of $K^o_S \rightarrow \pi^+\pi^-$ has been subtracted. Each value is an average over 2 GeV. The quoted errors are statistical only. The systematic uncertainty is less than 8%. The continuous line is the best fit to our data according to the formula $\langle n_{ch} \rangle = a + b \exp\left[c \sqrt{\ln(s/\Lambda^2)}\right]$. The dotted line is the best fit using PLUTO data. The dashed-dotted line is the (pp) total charged particle multiplicity. For this curve, the abscissa is $(\sqrt{s})_{pp}$. The open triangular points in this curve are our data using the standard way (i. e. without the subtraction of the leading proton effect) to calculate $\langle n_{ch} \rangle$ at fixed $(\sqrt{s})_{pp}$.

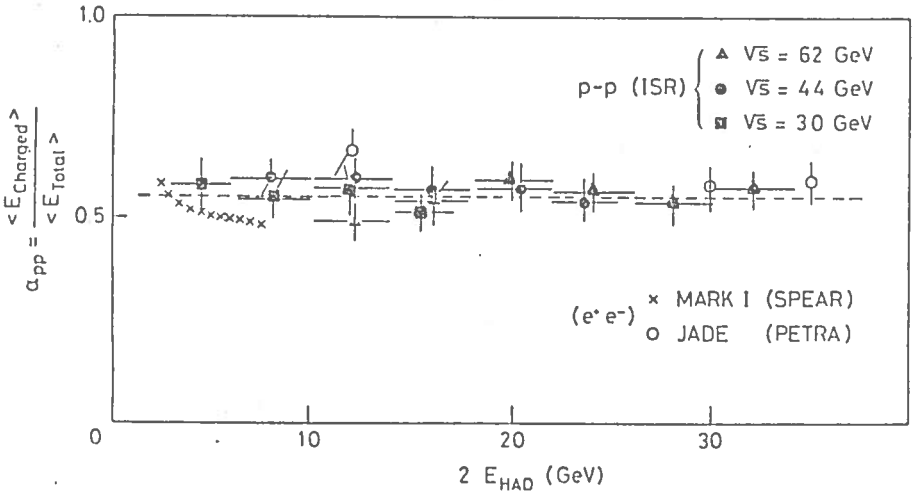

Fig. 44. The charged-to-total energy ratio obtained in (pp) collisions, α_{pp}, plotted versus $2E^{had}$ and compared with (e^+e^-) obtained at SPEAR and PETRA.

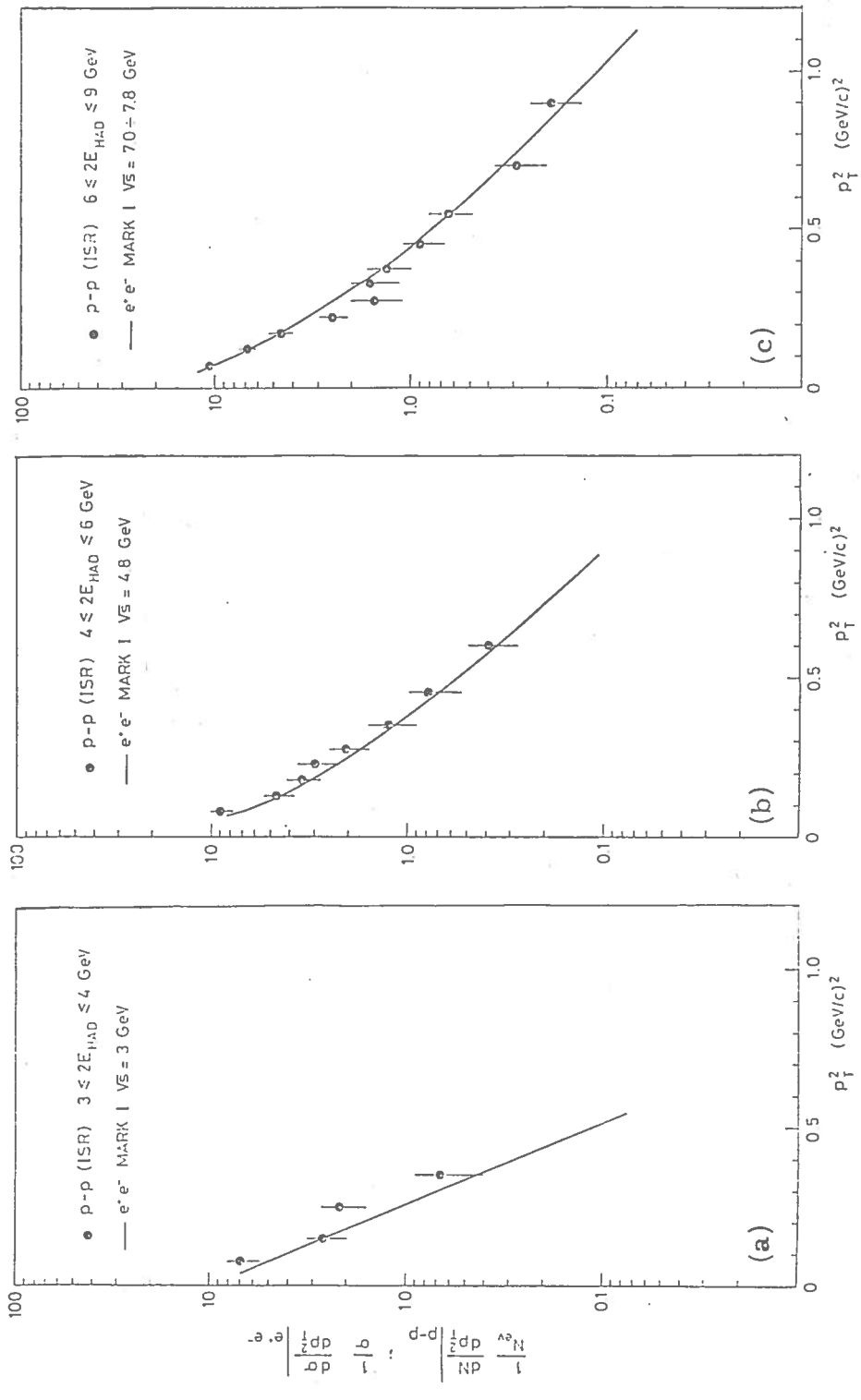

Fig. 45. The inclusive single-particle transverse momentum distribution $(1/N_{ev})(dN_{track}/dp_T^2)$ for data taken at $(\sqrt{s})_{pp} = 30$ GeV and for three intervals of $2E^{had}$: (a) $(3 \leq 2E^{had} \leq 4)$ GeV; (b) $(4 \leq 2E^{had} \leq 6)$ GeV; (c) $(6 \leq 2E^{had} \leq 9)$ GeV. Also shown is the fit to the SPEAR data at $(\sqrt{s})_{e^+e^-} = 3$, 4.8 and 7.4 GeV (continuous line).

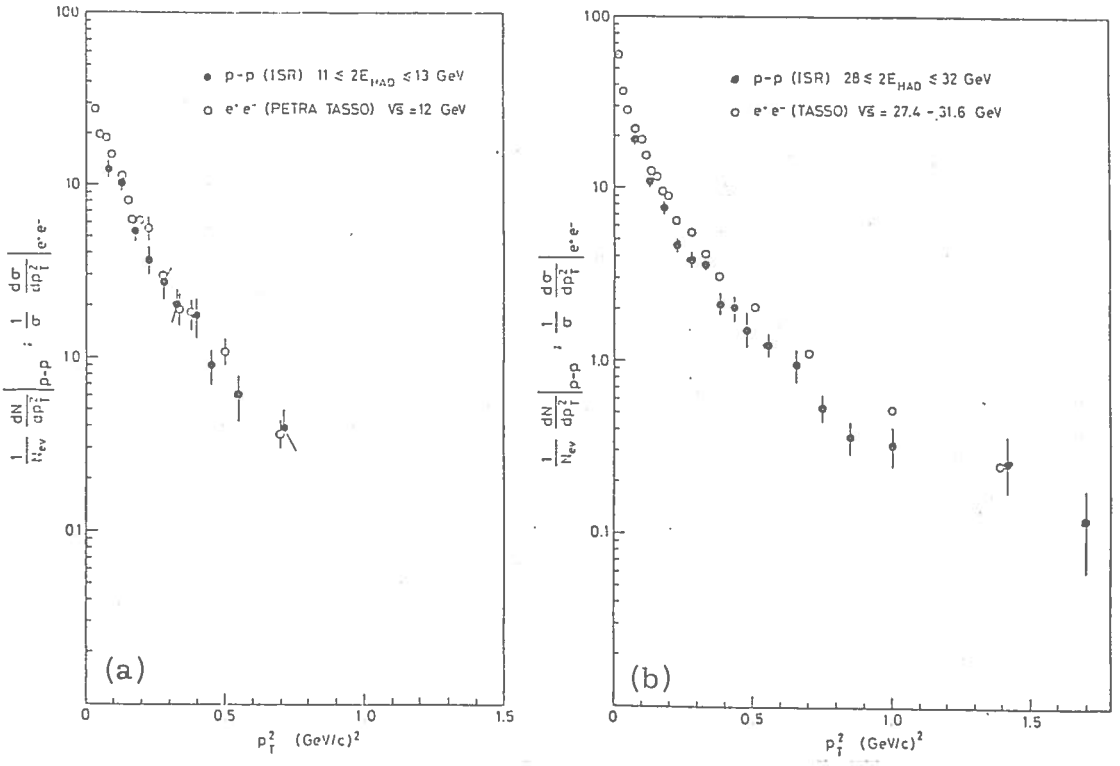

Fig. 46. The inclusive single particle transverse momentum distributions $(1/N_{ev})(dN_{track}/dp_T^2)$ for the following conditions: (a) $(11 \leq 2E^{had} \leq 13)$ GeV; (b) $(28 \leq 2E^{had} \leq 32)$ GeV). Also shown are data from TASSO at PETRA, relative to $(\sqrt{s})_{e^+e^-}$ = 12 and 27.4-31.6 GeV.

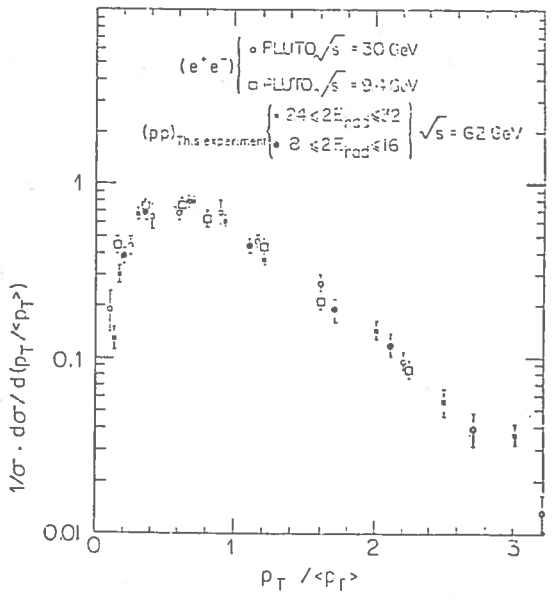

Fig. 47. The differential cross-section $(1/\sigma)[d\sigma/d(p_T/\langle p_T\rangle)]$ versus the "reduced" variable $p_T/\langle p_T\rangle$. These distributions allow a comparison of the multi particles systems produced in (e^+e^-) annihilation and in (pp) interactions in terms of the renormalized transverse momentum properties.

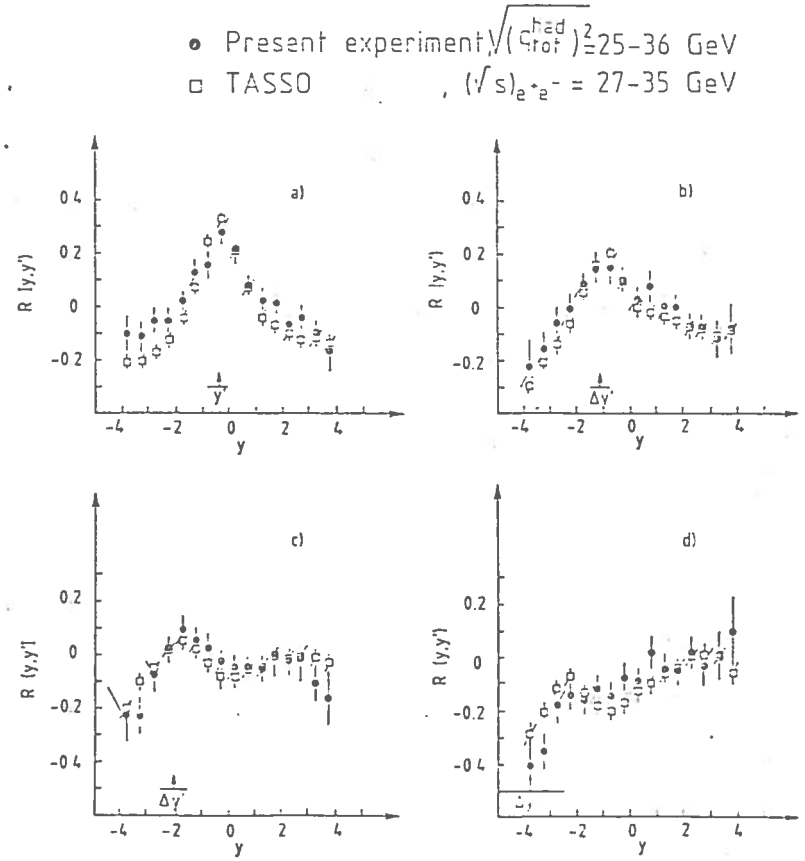

Fig. 48. Two particle-correlation in rapidity space: R(y,y'), for different y' intervals (a: $-0.75 \leq y' \leq 0$, b: $-1.5 \leq y' \leq -0.75$, c: $-2.5 \leq y' \leq -1.5$, d: $-5.5 \leq y' \leq -2.5$) as measured in the present experiment after the leading proton subtraction in the $\sqrt{(q_{tot}^{had})^2}$ range 25-36 GeV (black points), compared with the results by the TASSO collaboration at $(\sqrt{s})_{e^+e^-}$ between 27 and 35 GeV, as measured in (e^+e^-) annihilation (open squares).

collisions[31,32]. We have investigated this phenomenon and we have discovered that the "Leading" hadron effect is present no matter if the interaction is initiated by a hadron signal, or by a photon or by a weak boson (see Fig. 50). Moreover we have found that the "Leading" effect is more pronounced when more "quarks" are allowed to go from the initial to the final state (see Fig. 49). These findings imply that our new method of investigating multiparticle hadronic systems produced in (pp) interactions at the ISR is indeed of general validity and should be used in all reactions, in order to establish a common and understood basis for their comparison. It is manifestly uncorrect to compare processes where the "effective" energy available for particle production is not the same.

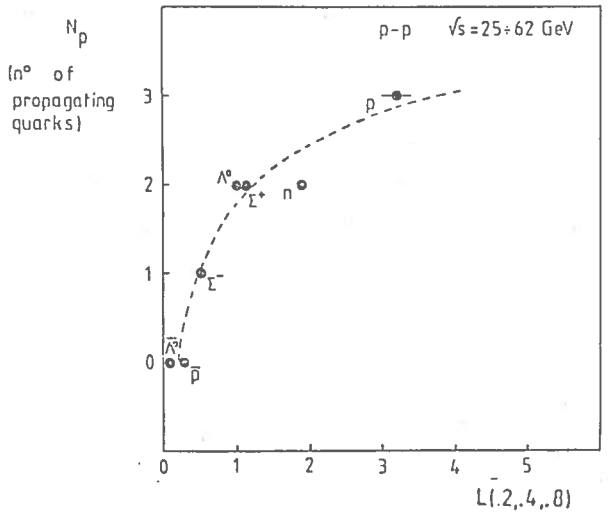

Fig. 49. The leading quantity L(0.2, 0.4, 0.8); for various final state hadrons in (pp) collisions at ISR energies (25-62 GeV), is plotted versus the number of propagating quarks from the incoming into the final-state hadrons. $L(x_0, x_1, x_2)$ is defined as

$$L(x_0, x_1, x_2) = \int_{x_1}^{x_2} F(x)\,dx \;/\; \int_{x_0}^{x_1} F(x)\,dx$$

where

$$F(x) = \frac{1}{\pi} \int \frac{2E}{\sqrt{s}} \frac{d^2\sigma}{dx\,dp_T^2}\, dp_T^2 \quad .$$

The dashed line is obtained by using a parametrization of the single-particle inclusive cross-section, as described in refs. 31, 32.

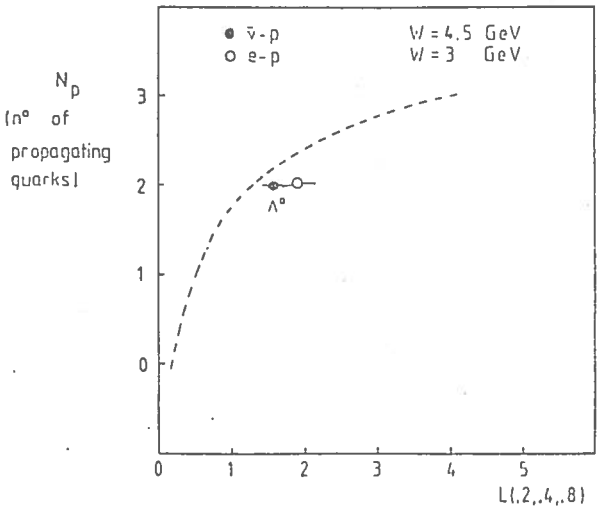

Fig. 50. L(0.2, 0.4, 0.8) for Λ^0 production in ($\bar{\nu}$p) and (ep) reactions. The dashed line is the same as for Fig. 49.

This means that, to compare for example the multiparticle hadronic systems produced in a (pp) collision at $(\sqrt{s})_{pp} = 30$ GeV with the multiparticle hadronic systems produced in a (e^+e^-) annihilation at $(\sqrt{s})_{e^+e^-} = 30$ GeV, is wrong. In fact $(\sqrt{s})_{pp}$ is not the "effective" energy available for particle production, while $(\sqrt{s})_{e^+e^-}$ is (see Fig. 42). In a (pp) interaction the effective energy available for particle production is $\sqrt{(q_{tot}^{had})^2}$, as shown in formula (9).

An analogous problem exists in the DIS case. Here the quantity W, defined as the total energy of the hadronic system, does indeed contain a "Leading" hadron. This is the reason why the average charged particle multiplicities measured in DIS and in (e^+e^-) could not agree (see Fig. 51).

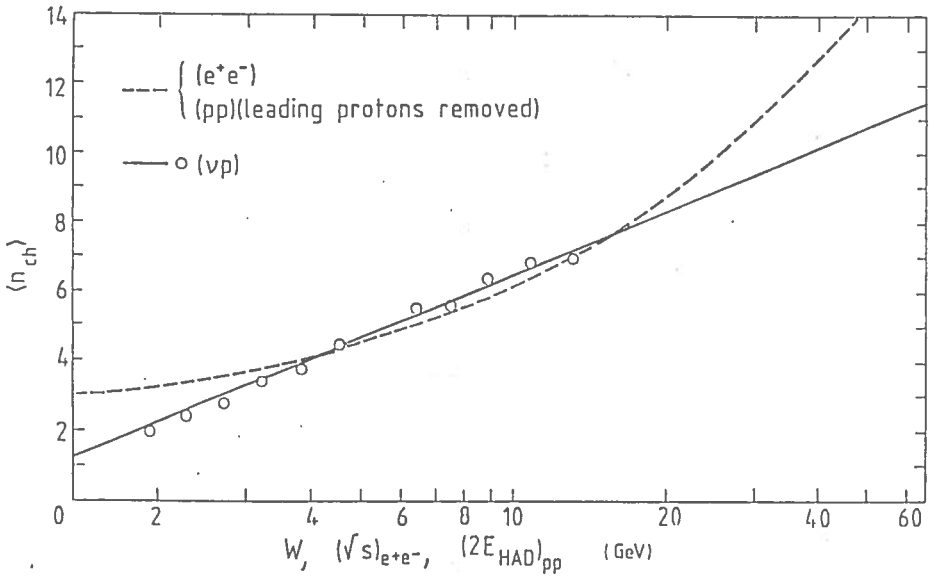

Fig. 51. The dashed line is the best fit to $\langle n_{ch} \rangle$ measured, in (e^+e^-) versus $(\sqrt{s})_{e^+e^-}$, and in (pp) removing leading protons versus $2E^{had}$. The points are the measurements of $\langle n_{ch} \rangle$ versus W in (νp) deep-inelastic scattering, and the continuous line is the best fit to these data.

The multiparticle hadronic system, produced in (e^+e^-) and DIS, can be compared, on a sound basis, only if $(\sqrt{s})_{e^+e^-}$ is compared not with W, but with $\sqrt{(q_{tot}^{had})^2}$.

3. 2. - The end of a myth: the high p_T physics.

So far the high p_T physics has had a highly privileged role in hadron phenomena. For example high p_T hadron physics was the only candidate to attempt a comparison with (e^+e^-) physics and DIS[59]. This

trend has been going on for a long time.

Recently the advent of QCD has emphasized the privileged role of the high p_T physics[60, 61, 62]. The reason is very simple: at high p_T, thanks to asymptotic freedom, QCD calculations can be attempted via perturbative methods and can be successfully confronted with experimental data. The new ($p\bar{p}$) Collider results are indeed the latest successful attempt in this trend[63, 64, 65].

On the contrary low p_T phenomena are "theoretically off limits", despite the fact that they represent an overwhelming amount of experimental data.

The crucial problem in order to understand the multihadronic systems produced is not to work at high p_T, but to identify the correct variables.

3. 3. - The identification of the correct variables.

Let me show how this is done.

a) e^+e^- annihilation is illustrated in the diagram below.

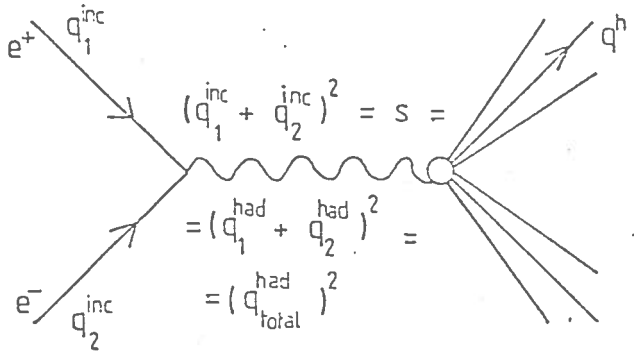

where q_1^{inc} and q_2^{inc} are the quadrimomenta of the incident electron e^-, and positron e^+. q^h is the quadrimomentum of a hadron produced in the final state, whose total energy is:

$$(\sqrt{s})_{e^+e^-} = \sqrt{(q_1^{inc} + q_2^{inc})^2} = 2E_{beam} \qquad (10)$$

(when the colliding beams have the same energy).
As we will see later,

$$q_1^{inc} = q_1^{had} , \qquad q_2^{inc} = q_2^{had}$$

where $q_{1,2}^{had}$ are the quadrimomenta available in a (pp) collisions for the production of a final state with total hadronic energy

$$\sqrt{(q_1^{had} + q_2^{had})^2} = \sqrt{(q_{tot}^{had})^2} . \qquad (11)$$

It is this quantity $\sqrt{(q_{tot}^{had})^2}$ which should be used in the comparison with (e^+e^-) annihilation, and therefore with $(\sqrt{s})_{e^+e^-}$. This means that

$$(\sqrt{s})_{e^+e^-} = \sqrt{(q_{tot}^{had})^2}\,. \tag{12}$$

Moreover, the fractional energy of hadron produced in the final state of an (e^+e^-) annihilation is given by

$$(x)_{e^+e^-} = 2\,\frac{q^h \cdot q_{tot}^{had}}{q_{tot}^{had} \cdot q_{tot}^{had}} = \frac{E^h}{(\sqrt{s})_{e^+e^-}}$$

where the dots indicate the scalar product and E^h is the energy of the hadron "h" measured in the (e^+e^-) c.m. system. Notice that the quadrimomentum q_{tot}^{had} has no space-like part:

$$q_{tot}^{had} \equiv \left\{ i0,\ (\sqrt{s})_{e^+e^-} \right\}.$$

b) DIS processes are illustrated in the diagram below:

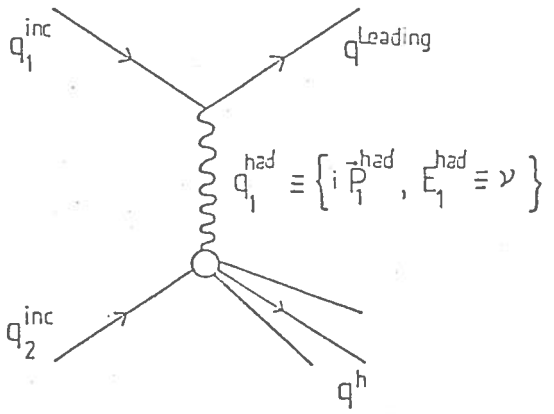

where q_1^{inc} and $q_1^{Leading}$ are the quadrimomenta of the initial and final state leptons, respectively, q_2^{inc} is the quadrimomentum of the target nucleon. q_1^{had} is the quadrimomentum transferred from the leptonic to the hadronic vertex whose time like component is usually indicated as ν,

$$q_1^{had} \equiv \{ iP_1^{had},\ \nu \equiv E_1^{had} \}.$$

Notice that, in order to easily identify the equivalent variables in (pp) interactions, we have introduced a notation in terms of E_1^{had} and P_1^{had}.

A basic quantity in DIS is the total hadronic mass

$$(W^2)_{DIS} = (q_1^{had} + q_2^{inc})^2$$

and the fractional energy

$$(z)_{DIS} = \frac{q^h \cdot q_2^{inc}}{q_1^{had} \cdot q_2^{inc}}$$

where again the dots between the quadrimomenta indicate their scalar product.

c) (pp) interactions are illustrated in the following graph:

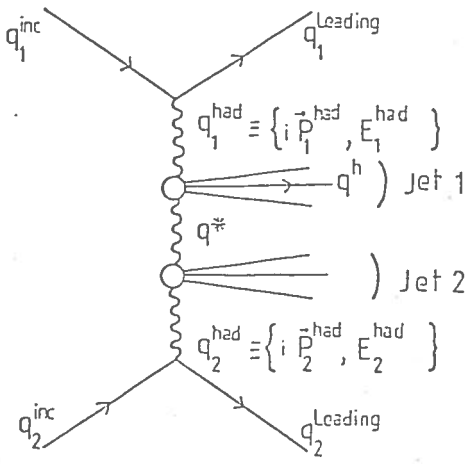

where $q_{1,2}^{inc}$ are the quadrimomenta of the two incident protons; $q_{1,2}^{Leading}$ are the quadrimomenta of the two leading protons. $q_{1,2}^{had}$ are the space-like quadrimomenta emitted by the two proton vertices. q^h is the quadrimomentum of a hadron produced in the final state.

Now, attention. A (pp) collision can be analyzed in such a way as to produce the key quantities proper to be compared with (e^+e^-) annihilation and DIS processes.

In fact, from the diagram above we can work out the following quantities needed if we want to compare (pp) physics with (e^+e^-) (notice that: $\sqrt{(q_{tot}^{had})^2} \simeq 2E^{had}$), i.e.

$$(q_{tot}^{had})_{pp} = (q_1^{had} + q_2^{had})_{pp}$$

in fact $\sqrt{(q^{had}_{tot})^2_{pp}} = (\sqrt{s})_{e^+e^-}$.

Moreover

$$(x)^{had}_{pp} = 2\,\frac{q^h \cdot q^{had}_{tot}}{q^{had}_{tot} \cdot q^{had}_{tot}}$$

to be compared with

$$(x)^{had}_{e^+e^-} = 2\,\frac{q^h \cdot (q^{had}_{tot})_{e^+e^-}}{(q^{had}_{tot})_{e^+e^-} \cdot (q^{had}_{tot})_{e^+e^-}}$$

where the subscripts (e^+e^-) in q^{had}_{tot} are in order to make it clear that these quantities are measured in (e^+e^-) collisions and are the quantities equivalent to q^{had}_{tot} measured in (pp) interactions.

The same (pp) diagram above can be used in order to work out the key quantities needed when we want to compare (pp) physics with DIS . In this case we have

$$(W^2)^{had}_{pp} = (q^{had}_1 + q^{inc}_2)^2$$

and

$$(z)^{had}_{pp} = \frac{q^h \cdot q^{inc}_2}{q^{had}_1 \cdot q^{inc}_2} \quad .$$

Notice that in (W^2) the leading proton n° 2 is not subtracted out. This is the reason for the differences found in the comparison between DIS and (e^+e^-) data (see Fig. 51). In fact (W^2) is not the effective total energy available for particle production, due to the presence in it of the leading proton.

3. 3. 1. - Experimental results.

A series of experimental results, where (pp) interactions have been analyzed "a' la" (e^+e^-) and "a' la" DIS have given impressive analogies in the multiparticle systems produced in these - so far considered - basically different processes : (pp), (e^+e^-), DIS.

The experimental data where (pp) interactions are compared with (e^+e^-) are shown in Figs. 40-48.

The experimental data where (pp) interactions are compared with DIS are shown in Figs. 51-54.

Notice the power of the (pp) interaction. Once this is analyzed in the correct way it produces results equivalent to (e^+e^-) and DIS .

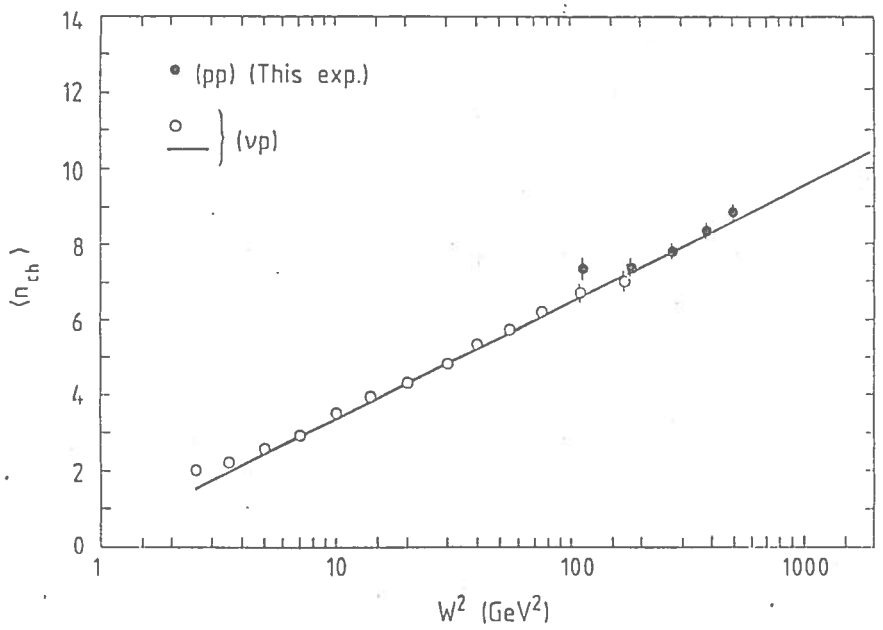

Fig. 52. The average charged particle multiplicities $\langle n_{ch} \rangle$ measured in (pp), at $(\sqrt{s})_{pp} = 30$ GeV, using a DIS-like analysis, are plotted versus W^2 (black points). The open points are the (νp) data and the continuous line is their best fit.

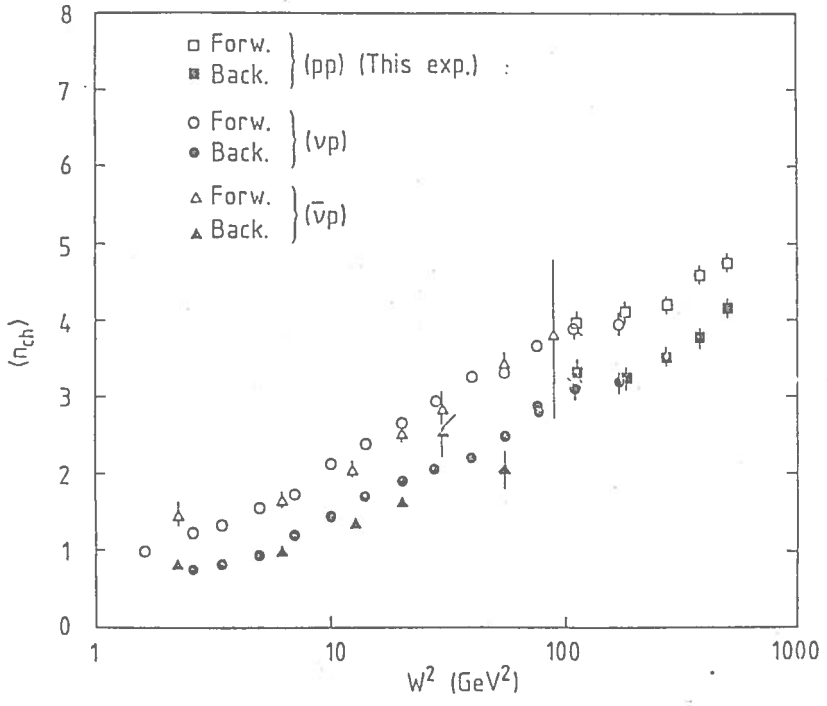

Fig. 53. The mean charged particle multiplicities $\langle n_{ch} \rangle_{F,B}$ in the forward and backward hemispheres versus W^2, in (νp), ($\bar{\nu}$p), and (pp) interactions.

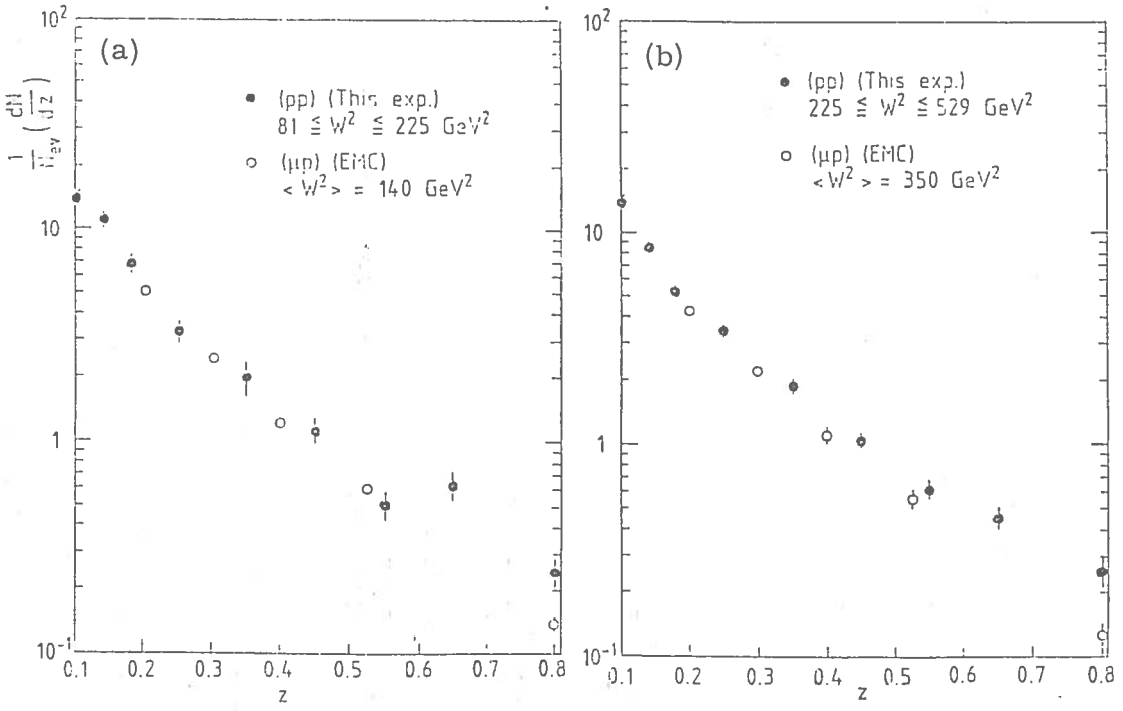

Fig. 54. The inclusive distribution of the fractional energy, z, for (pp) reactions: (a) in the energy interval $(81 \leq W^2 \leq 225)$ GeV^2 compared with the data from (μp) reactions at $\langle W^2 \rangle = 140$ GeV^2; (b) in the energy interval $(225 \leq W^2 \leq 529)$ GeV^2, compared with the data from (μp) reactions at $\langle W^2 \rangle = 350$ GeV^2.

This means that there is an important universality governing these - so far considered - different ways of producing multihadronic systems.

3. 3. 2. - Conclusions.

From the above analysis we can conclude:

1) The leading effect must be subtracted out if we want to compare purely hadronic interactions with (e^+e^-) and DIS.

2) The old myth based on the belief that in order to compare (pp) with (e^+e^-) and DIS, you need high p_T (pp) interactions, is over. In fact we have proved that low p_T (pp) interactions produce results in excellent agreement with (e^+e^-) annihilation and DIS processes. The basic parameter in (pp) interactions being $\sqrt{(q_{tot}^{had})^2}$ for a comparison with (e^+e^-), and W for a comparison with DIS.

The existence of high p_T events means that pointlike constituents exist inside the nucleon. But low p_T events contain the same amount of basic informations as high p_T events. No special features - apart from $\langle p_t \rangle$ (see point 3 below) - should emerge in the high p_T events because low p_T events follow (e^+e^-) and DIS.

3) Now two extrapolations.

There are two ways to produce $\sqrt{(q_{tot}^{had})^2}$:

i) one is at low p_T, and we have seen what happens ;

ii) the other is at high p_T : we have not been able to compare at constant values of $\sqrt{(q_{tot}^{had})^2}$ the multiparticle systems produced in (pp) interactions at high p_T and at low p_T.

Our analysis of the inclusive transverse momentum distribution, in terms of the renormalized variable $p_t/\langle p_t \rangle$, (notice that here p_t indicates the transverse momentum of the particles produced with respect to the jet axis, not to the colliding (pp) or ($p\bar{p}$) axis), is suggestive of a very interesting possibility : i. e. multiparticle systems produced at high p_T could show, at equivalent $\sqrt{(q_{tot}^{had})^2}$, higher values of $\langle p_t \rangle$. This would mean that high p_T multiparticle systems have a marked feature, the $\langle p_t \rangle$, which distinguishes them from the low p_T jets. This feature could be due to jets induced either by gluons or by heavy quarks.

An extrapolation of our method to the CERN ($p\bar{p}$) Collider in addition to the large energy jump, could allow to establish if this feature is or is not present in the high p_T jets.

Let us give an example. If two jets at the ($p\bar{p}$) Collider are produced back-to-back with the same transverse energy E_T, then we have

$$\sqrt{(q_{tot}^{had})^2} \cong 2E_T .$$

Suppose that we are at

$$2E_T = 100 \text{ GeV} .$$

This system, according to our extrapolation, should be like a multiparticle state produced by $(\sqrt{s})_{e^+e^-} = 100$ GeV.

The key point is to see if at the CERN ($p\bar{p}$) Collider a multiparticle system produced at low p_T but with the same value of $\sqrt{(q_{tot}^{had})^2}$, i. e.

$$\sqrt{(q_{tot}^{had})^2} = 100 \text{ GeV}$$

looks like the other one produced at high E_T. Let us emphasize, once again,that the main difference we can expect is the value of $\langle p_t \rangle$.

To recapitulate :

The new way of studying (pp) interactions, introduced by us more than three years ago[21], allows us to compare the multiparticle systems produced in a hadronic collider (like the ISR) with the multiparticle systems produced in a leptonic collider (like PETRA).

In other words, insofar as the multiparticle hadronic states are concerned, the ISR looks like an (e^+e^-) collider, whose energy goes

beyond the highest PETRA values. There is a difference between leptonic and baryonic machines : the production of open and hidden heavy flavour states. This difference can easily be accounted for in terms of the couplings which are just given by the up-like or down-like electric charges in the e^+e^- Colliders, while in the hadronic case the mass of the heavy flavours comes in with an inverse power law. But the structure of the multibody final states looks very similar at the ISR and at PETRA. Moreover if a lepton-hadron Collider would be built at equivalent ISR energies, the structure of the multibody final states would be identical, as shown by the comparison of the lowest energy ISR data with the highest energy (νp), ($\bar{\nu} p$) and (μp) scattering data.

A direct consequence of these findings is that the multibody hadronic final states produced at the CERN ($p\bar{p}$) Collider must follow our predictions.

4. - CONCLUSIONS

a) What have been observed at the ISR, in the production of heavy flavours, allows us to predict that the new heavy flavours, such as "top" and "superbeauty" at the CERN ($p\bar{p}$) Collider should be observable.

b) The detailed investigation of the properties of the multiparticle hadronic systems produced at the ISR, allows to establish a common basis between the production of particles in reactions : purely hadronic such as (pp) or ($p\bar{p}$) ; purely electromagnetic such as (e^+e^-) ; and semihadronic (such as Deep-Inelastic lepton-hadron processes). A consequence of these studies is the end of a celebrated myth : the high-p_T physics. Moreover, what is going to be observed at the ($\bar{p}p$) or (pp) future Colliders must follow our prediction.

c) The "New ISR Physics" is based on the above mentioned points. Both are very relevant in order to understand what is to be expected at extreme energies, i. e. those which are at present out of reach to (e^+e^-) Colliders, but are accessible to purely hadronic machines, as, for example, the CERN ($p\bar{p}$) Collider, the forthcoming Fermilab ($p\bar{p}$) Collider and the high-luminosity (pp) BNL Collider or possibly higher energy (pp) machines like the ELOISATRON[66].

REFERENCES

1. M. Basile et al., Nuovo Cimento 63A, 230 (1981).
2. M. Basile et al., Nuovo Cimento 62A, 14 (1981).
3. M. Basile et al., Lett. Nuovo Cimento 30, 487 (1981).
4. M. Basile et al., Lett. Nuovo Cimento 30, 481 (1981).
5. M. Basile et al., Lett. Nuovo Cimento 31, 97 (1981).
6. M. Basile et al., Nuovo Cimento 65A, 408 (1981).
7. M. Basile et al., Nuovo Cimento 65A, 457 (1981).
8. M. Basile et al., Nuovo Cimento 65A, 391 (1981).
9. M. Basile et al., Charm production at the CERN Intersecting Storage Rings Split Field Magnet, Proceedings of the XII Symposium on Multiparticle Dynamics, Notre Dame, Indiana, USA, June 21-26, 1981, page 799.
10. M. Basile et al., Beauty production at the CERN Intersecting Storage Rings Split Field Magnet, Proceedings of the XII Symposium on Multiparticle Dynamics, Notre Dame, Indiana, USA, June 21--26, 1981, page 815.
11. M. Basile et al., Charm production at the CERN Intersecting Storage Rings Split Field Magnet, Proceedings of the Intern. Conf. on High Energy Physics, Lisbon, Portugal, July 9-15, 1981, page 835.
12. M. Basile et al., Beauty production at the CERN Intersecting Storage Rings Split Field Magnet, Proceedings of the Intern. Conf. on High Energy Physics, Lisbon, Portugal, July 9-15, 1981, page 879.
13. M. Basile et al., Heavy flavour production at the highets energy (pp) interactions, Proceedings of the XIX Course of the "Ettore Majorana" Intern. School of Subnuclear Physics, Erice, Italy, July 31-August 11, 1981 : The Unity of the Fundamental Interactions, page 409.
14. M. Basile et al., Nuovo Cimento 67A, 40 (1982).
15. M. Basile et al., Lett. Nuovo Cimento 33, 33 (1982).
16. M. Basile et al., Lett. Nuovo Cimento 33, 17 (1982).
17. M. Basile et al., Nuovo Cimento 68A, 289 (1982).
18. M. Basile et al., Nuovo Cimento 68A, 65 (1982).
19. M. Basile et al., Charm and Beauty at the CERN ISR, Proceedings of the Moriond Workshop on New Flavours, Les Arcs, France, January 24-30, 1982, page 429.
20. M. Basile et al., New Flavours : experiment versus theory. From Charm to the 4^{th} Family, Invited Paper presented to the 3^{rd} Topical Workshop on Proton-Antiproton Collider Physics, Rome, Italy, January 12-14, 1983.
21. M. Basile et al., Phys. Letters 92B, 367 (1980).
22. M. Basile et al., Nuovo Cimento 58A, 193 (1980).
23. M. Basile et al., Phys. Letters 95B, 311 (1980).
24. M. Basile et al., Lett. Nuovo Cimento 29, 491 (1980).

25. M. Basile et al., Study of the basic properties of low p_t multiparticle systems produced in p-p collisions removing leading protons, Proceedings of the XX Intern. Conf. on High Energy Physics, Madison, Wisconsin, USA, July 17-23, 1980, page 86.
26. M. Basile et al., Phys. Letters 99B, 247 (1981).
27. M. Basile et al., Lett. Nuovo Cimento 30, 389 (1981).
28. M. Basile et al., Lett. Nuovo Cimento 31, 273 (1981).
29. M. Basile et al., Nuovo Cimento 65A, 400 (1981).
30. M. Basile et al., Nuovo Cimento 65A, 414 (1981).
31. M. Basile et al., Nuovo Cimento 66A, 129 (1981).
32. M. Basile et al., Lett. Nuovo Cimento 32, 321 (1981).
33. M. Basile et al., Lett. Nuovo Cimento 32, 210 (1981).
34. M. Basile et al., Preprint CERN-EP/81-147 (1981).
35. M. Basile et al., Low-p_t proton-proton collisions at the CERN Intersecting Storage Rings, Proceedings of the XII Symposium on Multiparticle Dynamics, Notre Dame, Indiana, USA, June 21-26, 1981, page 717.
36. M. Basile et al., Low-p_t proton-proton collisions at the CERN Intersecting Storage Rings, Proceedings of the Intern. Conf. on High Energy Physics, Lisbon, Portugal, July 9-15, 1981, page 924.
37. M. Basile et al., What can we learn from high-energy, soft (pp) interactions, Proceedings of the XIX Course of the "Ettora Majorana" Intern. School of Subnuclear Physics, Erice, Italy, July 31-August 11, 1981, page 695.
38. M. Basile et al., Nuovo Cimento 67A, 53 (1982).
39. M. Basile et al., Nuovo Cimento 67A, 244 (1982).
40. M. Basile et al., Preprint CERN-EP/82-182 (1982), submitted to Nuovo Cimento.
41. M. Basile et al., Lett. Nuovo Cimento 36, 303 (1983).
42. G. Bonvicini et al., Preprint CERN-EP/83-29 (1983), submitted to Lett. Nuovo Cimento.
43. G. Bonvicini et al., Preprint CERN-EP/83-33 (1983), submitted to Lett. Nuovo Cimento.
44. G. Bonvicini et al., Preprint CERN-EP/83-42 (1983), submitted to Lett. Nuovo Cimento.
45. J. Berbiers et al., Preprint CERN-EP/83-44 (1983), submitted to Lett. Nuovo Cimento.
46. M. Basile et al., Hadron colliders versus (e^+e^-) colliders: a contribution to the round table from the BCF group, Invited Paper presented to the 3rd Topical Workshop on Proton-Antiproton Collider Physics, Rome, Italy, January 12-14, 1983.
47. S. Ferrara, private communication.
48. A. Martin, The masses of the Heavy Flavoured Hadrons, CERN Preprint TH-3314 (1982).

49. D. Drijard et al., Phys. Letters 85B, 452 (1979); K. Giboni et al., Phys. Letters 85B, 437 (1979); W. Lockman et al., Phys. Letters 85B, 443 (1979); J. Eickmeyer et al., XX ICHEP (Madison, 1981); D. Drijard et al., Phys. Letters 81B, 250 (1979); P. F. Jacques et al., Phys. Rev. D21, 1206 (1980); P. Coteus et al., Phys. Rev. Letters 42, 1438 (1979); A. Soukas et al., Phys. Rev. Letters 44, 564 (1980); A. E. Asratyan et al., Phys. Letters 74B, 497 (1978); P. Alibran et al., Phys. Letters 74B, 134 (1978); T. Hansl et al., Phys. Letters 74B, 139 (1978); A. Bosetti et al., Phys. Letters 74B, 143 (1978); M. Fritze et al., Phys. Letters 96B, 427 (1980); D. Jonker et al., Phys. Letters 96B, 435 (1980); H. Abramowicz et al., CERN Preprint CERN-EP/82-17 (1982); M. Aguilar-Benitez et al., CERN Preprint CERN-EP/81-131 (1981); T. Aziz et al., Nuclear Phys. B199, 424 (1982); J. Sandweiss et al., Phys. Rev. Letters 44, 1104 (1980).
50. F. Halzen, W. Y. Keung and D. M. Scott, Madison Report MAD/PH/63 (1982).
51. R. Odorico, Phys. Letters 107B, 231 (1981).
52. V. Barger, F. Halzen and W. Y. Keung, Phys. Rev. D24, 1428 (1981).
53. J. Badier et al., XXI Intern. Conf. on High Energy Physics, Paris, 1982.
54. K. Chadwick et al., Preprint CLNS/82/546 (1982).
55. F. Halzen, Rapp. Talk, XXI Intern. Conf. on High Energy Physics, Paris, 1982.
56. L. Olsen, Moriond Workshop on New Flavours, Les Arcs, France, 1982.
57. G. Arnison et al., UA1 Collaboration, Preprint CERN-EP/82-171 (1982).
58. G. Arnison et al., UA1 Collaboration, Preprint CERN-EP/83-13 (1983).
59. M. Jacob and P. V. Landshoff, Phys. Rep. 48, nº 4 (1978).
60. E. Reya, Phys. Rep. 69, nº 3 (1981).
61. P. V. Landshoff, PRE-25972.
62. M. Jacob, Preprint CERN-TH/3515.
63. UA2 Collaboration, Phys. Letters B118, 203 (1982).
64. UA1 Collaboration, Preprint CERN-EP/83-002 (1983).
65. H. Boggild, Preprint CERN-EP/82-187 (1982).
66. A. Zichichi, ELOISATRON. The European Long Intersecting Storage Accelerator, Galilei and Nobel Symposia, San Remo and Rome, 1-11 May 1983.